Multiobjective Best Theory Diagrams for cross-ply composite plates employing polynomial, zig-zag, trigonometric and exponential thickness expansions

Multiobjective Best Theory Diagrams for Cross-Ply Composite Plates employing Polynomial, Zig-Zag, Trigonometric and Exponential Thickness Expansions

J. Yarasca [a], J. L. Mantari [a,b], M. Petrolo [c], E. Carrera [c]

a Faculty of Mechanical Engineering, Universidad de Ingeniería y Tecnología (UTEC), Medrano Silva 165, Barranco, Lima, Peru

b University of New Mexico, Department of Mechanical Engineering, Albuquerque, New Mexico, U.S.A.

c MUL^2 Group, Department of Mechanical and Aerospace Engineering, Politecnico di Torino, Corso Duca degli Abruzzi 24, 10129 Torino, Italy

** This manuscript has not been published elsewhere and that it has not been submitted simultaneously for publication elsewhere.

Abstract

This paper presents Best Theory Diagrams (BTDs) for plates considering all the displacement and stress components as objectives. The BTD is a diagram in which the minimum number of terms that have to be used to achieve the desired accuracy can be read. Maclaurin, zig-zag, trigonometric and exponential expansions are employed for the static analysis of cross-ply composite plates. The Equivalent Single Layer (ESL) approach is considered, and the Unified Formulation developed by Carrera is used. The governing equations are derived from the Principle of Virtual Displacement (PVD), and Navier-type closed form solutions are adopted. BTDs are obtained using the Axiomatic/Asymptotic Method (AAM) and genetic algorithms (GA). The results show that the BTD can be used as a tool to assess the accuracy and computational efficiency of any structural models and to draw guidelines to develop structural models. The inclusion of the multiobjective capability extends the BTD validity to the recognition of the role played by each output parameter in the refinement of a structural model.

Keywords: Plates; Carrera Unified Formulation (CUF); Zig-Zag; Trigonometric; Exponential; Best Theory Diagram; Composite Structures.

1. Introduction

Composite laminated plates are increasingly common in many engineering applications, such as aerospace, mechanical, marine and civil structures. In fact, composite plates have many favorable mechanical properties, e.g. high stiffness, and low density. The high demand for the use of composite material structures calls for research of efficient and accurate numerical techniques to predict the structural and dynamical behavior of laminated composites.

Classical plate theories (CPT) neglect transverse shear and normal stresses [1, 2]. An extension of this model to multi-layered structures is referred to as the Classical Lamination Theory (CLT) [3, 4]. Due to the increasing use of thick laminated plates in structures, Reissner and Mindlin [5, 6] included transverse shear effects in their well-

known First-Order Shear Deformation Theory (FSDT). Although the FSDT is simple to implement and apply for both thick and thin laminated plates, the accuracy strongly depends on shear correction factors and the nonexistence of complicated stress gradients [7]. The limitations of the FSDT weaken or disappear with Higher-order Shear Deformation Theories (HSDT). The HSDTs assume quadratic, cubic, higher variations or non-polynomial terms to improve the displacement field along the thickness direction [8-14]. Further enhancements are useful if local effects are important or accuracy in the calculation of the transverse stresses is required. The zig-zag models [15, 16] and mixed variational tools [17] can deal with these phenomena.

Plate modeling has two main approaches, the Equivalent Single Layer (ESL) and the Layer-Wise (LW) models [18-22]. Theories based on the ESL assumption offer reduced computational complexity; however, they struggle to model the zig-zag effects typical of laminates. LW theories have quasi-three-dimensional predictive capabilities; however, the computational effort can increase significantly.

The present paper makes use of ESL models and includes non-polynomial terms to Maclaurin expansions. Different non-polynomial kinematics models have been proposed in the literature. Shimpi and Ghugal [12] proposed a LW trigonometric shear deformation theory for the analysis of composite beams. Arya et al. [13] developed a zig-zag model using a sine term to represent the non-linear displacement field across the thickness in symmetrically laminated beams. Mantari and co-workers have recently proposed various extensions to non-polynomial plate models, including ESL and LW trigonometric models [23, 24], HSDTs based on Trigonometric-Exponential terms [25, 26], hybrid Maclaurin-trigonometric models [27, 28], a generalized hybrid formulation for the study of functionally graded sandwich beams [29, 30]. Nguyen et al. [31] developed a unified framework on HSDTs for laminated composite plates. The Carrera

Unified Formulation (CUF) has been recently employed to develop non-polynomial structural models [32-37].

The refined models employed in this paper are based on the CUF. According to CUF, the governing equations are given via the so-called fundamental nuclei whose form does not depend on either the expansion order nor on the choices made for the base functions to generate any structural model [38-40]. In the CUF framework, Carrera and Petrolo [41, 42] introduced the Axiomatic/Asymptotic Method (AAM) to develop reduced models whose accuracies are equivalent to those of full higher-order models. The AAM has been applied to several problems, including: static and free vibration of beams [41, 43], metallic and composite plates [42, 44], shells [45, 46], LW models [47, 48], advanced models based on the Reissner Mixed Variational Theorem [49], piezoelectric plates [50], and thermomechanical problems [51].

The AAM has led to the BTD [52]. The BTD allows one to determine the minimum number of expansion terms - i.e. unknown variables - required to meet a given accuracy; or, conversely, the best accuracy provided by a given amount of variables. To construct BTDs with a lower computational cost, a genetic algorithm was employed by Carrera and Miglioretti [53]. In particular, BTDs were built by minimizing the number of the expansion terms and the error on an output parameter, such as a displacement or stress component. Petrolo et al. [54] presented BTDs for ESL and LW composite plate models based on Maclaurin and Legendre polynomial expansions of the unknown variables along the thickness. Recently, Carrera et al. have recently extended the BTD to multifield problems [55].

The present work presents a method to develop BTDs considering multiple objectives simultaneously; in particular, the three displacement components and the six stress ones. The BTDs are therefore the Pareto fronts of the optimization of the

expansions to minimize the error on each displacement and stress component. A Maclaurin expansion with zig-zag terms and a hybrid Maclaurin, zig-zag, trigonometric and exponential expansion are considered. The non-polynomial terms in the latter are selected according to Filippi et al. [36].

The present paper is organized as follows: a description of the adopted formulation is provided in Section 2; the governing equations and closed-form solution is presented in Section 3; the AAM is presented in Section 4; the BTD for multiple output parameters is introduced in Section 5; the results are presented in Section 6, and the conclusions are drawn in Section 7.

2. Carrera Unified Formulation for Plates

The geometry and the coordinate system of the multilayered plate are shown in Fig. 1, where *x* and *y* are the in-plane coordinates while *z* is the thickness coordinate. The integer *k* denotes the layer number. In the framework of the CUF, the displacement components of a plate model is

$$\boldsymbol{u}(x,y,z) = F_\tau(z) \cdot \boldsymbol{u}_\tau(x,y) \qquad \tau = 1, 2, \dots., N+1 \tag{1}$$

where $\boldsymbol{u}$ is the displacement vector (u_x, u_y, u_z). F_τ are the expansion functions. $\boldsymbol{u}_\tau$ $(u_{x_\tau}, u_{y_\tau}, u_{z_\tau})$ is the vector of the displacements variables. In the ESL case, F_τ functions can be Maclaurin functions of *z* defined as $F_\tau = z^{\tau-1}$. The ESL models are referred to as EDN, where N is the expansion order. An example of an ED4 displacement field is

$$u_x = u_{x_1} + z\,u_{x_2} + z^2 u_{x_3} + z^3 u_{x_4} + z^4 u_{x_5}$$

$$u_y = u_{y_1} + z\,u_{y_2} + z^2 u_{y_3} + z^3 u_{y_4} + z^4 u_{y_5}$$

$$u_z = u_{z_1} + z\,u_{z_2} + z^2 u_{z_3} + z^3 u_{z_4} + z^4 u_{z_5} \tag{2}$$

The ESL models considering the zig-zag functions are indicated as EDZN. The components of an EDZ4 plate model are:

$$u_x = u_{x_1} + z\,u_{x_2} + z^2 u_{x_3} + z^3 u_{x_4} + z^4 u_{x_5} + (-1)^k \zeta_k u_{x_6}$$

$$u_y = u_{y_1} + z\,u_{y_2} + z^2 u_{y_3} + z^3 u_{y_4} + z^4 u_{y_5} + (-1)^k \zeta_k u_{y_6}$$

$$u_z = u_{z_1} + z\,u_{z_2} + z^2 u_{z_3} + z^3 u_{z_4} + z^4 u_{z_5} + (-1)^k \zeta_k u_{z_6} \tag{3}$$

The present paper investigates the influence of trigonometric, exponential and zig-zag terms in ESL models. Two different plate theories are compared, the EDZ4 model presented in Eq. (3) and the EDZ17 model reported in Table 1. The displacement field of EDZ17 consists of 54 unknown variables, which include 15 Maclaurin terms, three zig-zag terms - the EDZ4 terms -, 24 trigonometric terms and 12 exponential terms. For instance, the full expression of the displacement along *x* is

$$u_x = u_{x_1} + z\,u_{x_2} + z^2 u_{x_3} + z^3 u_{x_4} + z^4 u_{x_5} + (-1)^k \zeta_k u_{x_6} + \sin\left(\frac{\pi z}{h}\right) u_{x_7}$$

$$+ \sin\left(\frac{2\pi z}{h}\right) u_{x_8} + \sin\left(\frac{3\pi z}{h}\right) u_{x_9} + \sin\left(\frac{4\pi z}{h}\right) u_{x_{10}} + \cos\left(\frac{\pi z}{h}\right) u_{x_{11}} +$$

$$\cos\left(\frac{2\pi z}{h}\right) u_{x_{12}} + + \cos\left(\frac{3\pi z}{h}\right) u_{x_{13}} + \cos\left(\frac{4\pi z}{h}\right) u_{x_{14}} + e^{\frac{z}{h}} u_{x_{15}}$$

$$+ e^{\frac{2z}{h}} u_{x_{16}} + e^{\frac{3z}{h}} u_{x_{17}} + e^{\frac{4z}{h}} u_{x_{18}} \tag{4}$$

where *h* is the thickness of the plate.

3. Governing equations and Closed-form solution

Geometrical relations enable to express the in-plane $\boldsymbol{\epsilon}_p^k$ and the out-planes $\boldsymbol{\epsilon}_n^k$ strains in terms of the displacement $\boldsymbol{u}$,

$$\boldsymbol{\epsilon}_p^k = \left[\epsilon_{xx}^k,\ \epsilon_{yy}^k,\ \epsilon_{xy}^k\right]^T = \left(\boldsymbol{D}_p^k\right)\boldsymbol{u}^k,\ \ \boldsymbol{\epsilon}_n^k = \left[\epsilon_{xz}^k,\ \epsilon_{yz}^k,\ \epsilon_{zz}^k\right]^T = \left(\boldsymbol{D}_{np}^k + \boldsymbol{D}_{nz}^k\right)\boldsymbol{u}^k \quad (5)$$

where $\boldsymbol{D}_p^k$, $\boldsymbol{D}_{np}^k$ and $\boldsymbol{D}_{nz}^k$ are differential operators whose components are:

$$\boldsymbol{D}_p^k = \begin{bmatrix} \frac{\partial}{\partial x} & 0 & 0 \\ 0 & \frac{\partial}{\partial y} & 0 \\ \frac{\partial}{\partial y} & \frac{\partial}{\partial x} & 0 \end{bmatrix}, \quad \boldsymbol{D}_{np}^k = \begin{bmatrix} 0 & 0 & \frac{\partial}{\partial x} \\ 0 & 0 & \frac{\partial}{\partial y} \\ 0 & 0 & 0 \end{bmatrix}, \quad \boldsymbol{D}_{nz}^k = \begin{bmatrix} \frac{\partial}{\partial z} & 0 & 0 \\ 0 & \frac{\partial}{\partial z} & 0 \\ 0 & 0 & \frac{\partial}{\partial z} \end{bmatrix} \quad (6)$$

Stress components for a generic *k* layer can be obtained using the constitutive law,

$$\boldsymbol{\sigma}_p^k = \boldsymbol{C}_{pp}^k\boldsymbol{\epsilon}_p^k + \boldsymbol{C}_{pn}^k\boldsymbol{\epsilon}_{\boldsymbol{n}}^k$$

$$\boldsymbol{\sigma}_n^k = \boldsymbol{C}_{np}^k\boldsymbol{\epsilon}_p^k + \boldsymbol{C}_{nn}^k\boldsymbol{\epsilon}_{\boldsymbol{n}}^k \quad (7)$$

where $\boldsymbol{C}_{pp}^k$, $\boldsymbol{C}_{pn}^k$, $\boldsymbol{C}_{np}^k$ and $\boldsymbol{C}_{nn}^k$ are:

$$\boldsymbol{C}_{pp}^k = \begin{bmatrix} C_{11}^k & C_{12}^k & C_{16}^k \\ C_{12}^k & C_{22}^k & C_{26}^k \\ C_{16}^k & C_{26}^k & C_{66}^k \end{bmatrix}, \qquad \boldsymbol{C}_{pn}^k = \begin{bmatrix} 0 & 0 & C_{13}^k \\ 0 & 0 & C_{23}^k \\ 0 & 0 & C_{36}^k \end{bmatrix},$$

$$\boldsymbol{C}_{np}^k = \begin{bmatrix} 0 & 0 & 0 \\ 0 & 0 & 0 \\ C_{13}^k & C_{23}^k & C_{36}^k \end{bmatrix}, \qquad \boldsymbol{C}_{nn}^k = \begin{bmatrix} C_{55}^k & C_{45}^k & 0 \\ C_{45}^k & C_{44}^k & 0 \\ 0 & 0 & C_{33}^k \end{bmatrix}, \quad (8)$$

For the sake of brevity, the dependence of the elastic coefficients C_{ij}^k on Young's modulus, Poisson's ratio, the shear modulus, and the fiber angle is not reported. They can be found in [9]. The analysis of a plate can be conducted using the principle of virtual displacement (PVD),

$$\delta L_{int} = \delta L_{ext} \quad (9)$$

Where δL_{int} is the virtual variation of the internal work and δL_{ext} is the virtual variation of the work made by the external loadings. The PVD can be written as

$$\sum_{k=1}^{N_l} \int_V \left(\delta \boldsymbol{\epsilon}_p^k \boldsymbol{\sigma}_p^k + \delta \boldsymbol{\epsilon}_n^k \boldsymbol{\sigma}_n^k\right) dV = \sum_{k=1}^{N_l} \delta L_{ext}^k \tag{10}$$

Further details about the CUF and its implementation through the use of variational principles can be found in [40]. The governing equations are expressed in compact form,

$$\delta \boldsymbol{u}_s^k: \ \boldsymbol{K}_d^{k\tau s} \boldsymbol{u}_\tau^k = \boldsymbol{P}_s^k \tag{11}$$

Where $\boldsymbol{P}_\tau^k$ is the external load. The fundamental nucleus, $\boldsymbol{K}_d^{k\tau s}$, is assembled through the indexes τ and s to obtain the stiffness matrix of each layer k. The matrices of each layer are assembled at the multilayer level according to the approach considered, for this work the ESL approach is adopted.

The numerical results were obtained via the Navier closed-form solution for simply supported orthotropic plates, loaded by a transverse distribution of harmonic loadings. The following properties hold:

$$C_{16} = C_{26} = C_{36} = C_{45} = 0 \tag{12}$$

The displacements are expressed in the following harmonic form,

$$u_x = \sum_{m,n} U_x \cdot cos\left(\frac{m\pi x}{a}\right) sin\left(\frac{n\pi y}{b}\right)$$

$$u_y = \sum_{m,n} U_y \cdot sin\left(\frac{m\pi x}{a}\right) cos\left(\frac{n\pi y}{b}\right)$$

$$u_z = \sum_{m,n} U_z \cdot sin\left(\frac{m\pi x}{a}\right) sin\left(\frac{n\pi y}{b}\right) \tag{13}$$

where U_x, U_y, and U_z are the amplitudes, m and n are the wave numbers, and a and b are the dimensions of the plate in the x and y directions, respectively.

4. Axiomatic/Asymptotic Method

The introduction of higher-order terms in a plate model offers significant advantages in terms of improved structural response prediction at the expense of higher computational costs. The axiomatic/asymptotic method (AAM) allows us to lower the computational cost of a model without affecting its accuracy. A typical AAM analysis has the following steps:

(1) Parameters such as geometry, boundary conditions, loadings, materials, and stacking sequences are fixed.
(2) A set of output parameters is chosen, such as displacement and stress components.
(3) A theory is fixed; that is, the displacement variables to be analyzed are defined.
(4) A reference solution is defined; in the present work, a fourth-order LW model (LD4) is adopted.
(5) The CUF is used to generate the governing equations for the considered theories.
(6) A penalty technique allows the deactivation of each variable in turn.
(7) Reduced models are built using combinations of the full model variables, and their accuracy is evaluated. All those variables that do not affect the accuracy are discarded.
(8) The most efficient kinematic model for a given structural problem is then obtained by discarding all the noneffective displacement variables.

A graphical notation is introduced to represent the results. This consists of a table in which rows are related to the three displacement components, and the number of

columns is equal to the number of the displacement variables used in the expansion. As an example, an ED4 model (full model) and a reduced model in which the term u_{x_2} is deactivated is shown in Table 2. The meaning of the symbols ▲ and Δ is reported in Table 3. The reduced displacement field of Table 2 is

$$u_x = u_{x_1} + \qquad z^2 u_{x_3} + z^3 u_{x_4} + z^4 u_{x_5}$$

$$u_y = u_{y_1} + z\, u_{y_2} + z^2 u_{y_3} + z^3 u_{y_4} + z^4 u_{y_5}$$

$$u_z = u_{z_1} + z\, u_{z_2} + z^2 u_{z_3} + z^3 u_{z_4} + z^4 u_{z_5} \tag{14}$$

5. Best Theory Diagram

The construction of refined models through the AAM allows one to obtain a diagram in which each refined model is associated with the number of active terms and the error on a given displacement or stress output variable on a reference solution. Best models are those that, for a given error, require the minimum number of variables; or, for a given number of variables, provide the best accuracy. Best models represent a Pareto front of an optimization problem in which the objectives are the minimization of the error and the number of terms, as shown in [53, 54]. Such a Pareto front is the BTD. In previous works, only one displacement or stress component was considered; that is, the best models were found considering the accuracy in only one output variable. In this paper, for the first time, BTDs are built considering multiple displacement and stress outputs.

BTDs could be obtained directly from the AAM without employing an optimization tool. The computational cost required for the BTD construction via the AAM depends on the number of unknown variables in the model. The number of all possible combinations of active/not-active terms for a given model is equal to 2^M, where M is the number of unknown variables (DOFs) in the model. In the cases considered in this paper, M is equal

to 18 and 54 for the EDZ4 and EDZ17, respectively. The resulting computational cost to build the BTD is, therefore, excessive.

A way to build the Pareto front is to rank the refined models according to a dominance rule. This ranking is based on the principle of non-dominated sorting (Pareto dominance). Models in the Pareto front are those for which the improvement in one objective implies the worsening of at least one other objective. All the non-dominated models are added to the Pareto front. The selection of the refined models which belong to the Pareto front can be stated as an *N*-dimensional minimization problem, where *N* is the number of objective functions. It is clear that, as *N* increases, the number of refined models in the Pareto front increments considerably. This may cause complications in the selection of an appropriately refined model. To simplify the analysis from *N* to a three-dimensional minimization problem, the following objective functions were chosen:

- The number of terms in the refined model.
- The mean error of the output parameters (μ).
- The standard deviation of the output parameters (σ).

By minimizing these three objectives, one can build a Pareto front which includes refined models with least unknown variables, minimum error, and minimum standard deviation. The refined models in the Pareto front define a surface in the 3D solution space, as presented in Fig. 2. Due to the large number of best plate theories in the Pareto front, the selection of a plate model is still more complicate than the case with a single output parameter. To facilitate the selection of refined models in the Pareto front a new metric, denoted as $\%Error_{ul}$ (see Fig. 4), was introduced. $\%Error_{ul}$ is equal to the sum of the mean error and the standard deviation and is a measure of the upper limit of the error of each output parameter considered. It is important to remark that $\%Error_{ul}$ is not exactly

the upper limit error of the output parameters, but an indicator employed for comparative purposes. The new 2D Pareto front is built selecting the best plate theories from the 3D one and considering the following new objective functions:

- The number of terms in a refined model.
- $\%Error_{ul}$.

The computational cost of this further optimization is not significant since the optimization is carried out on a very small set of refined models.

As proved by Carrera and Miglioretti [53], a genetic algorithm can be used to build a BTD. A solution vector $\boldsymbol{x} \in \boldsymbol{X}$, where $\boldsymbol{X}$ is the solution space, is called an individual or chromosome. Chromosomes are made of discrete units called genes. Each gene controls one or more features of the individual. GAs operate with a collection of chromosomes, called a population. The population is normally randomly initialized. As the search evolves, the population includes fitter and fitter solutions, and eventually it converges, meaning that it is dominated by a single solution. Simple GAs use three operators to generate new solutions from existing ones: reproduction, crossover, and mutation. On the reproduction, individuals with higher fitness are preserved for the next generation. Each individual has a fitness value based on its rank in the population. The population is ranked according to a dominance rule. The fitness of each chromosome is evaluated through the following formula:

$$r_i(\boldsymbol{x_i}, t) = 1 + nq(\boldsymbol{x_i}, t) \tag{15}$$

where $nq(\boldsymbol{x}, t)$ is the number of solutions dominating $\boldsymbol{x}$ at generation *t*. A lower rank corresponds to a better solution. To maintain diversity among non-dominated solutions, niching among solutions of each rank is employed as shown in Ref. [56]. On the

crossover, two chromosomes called parents, are combined to form new chromosomes, called offsprings. This operator allows the GA to find new solutions. The mutation operator introduces random changes at the gene level, with the aim of recovering strong genes possibly loss on the crossover operation. In this paper, an elitism technique is employed to preserve the dominant individuals in each generation without any changes in its configuration. A complete explanation of genetic algorithms can be found in Refs. [56,57].

In the present work, each plate theory has been considered as an individual. The genes are the terms of the expansion along the thickness of the three displacement fields in the following manner. Each gene can be active or not, the deactivation of a term is obtained by exploiting a penalty or row-column elimination technique. The representation of this method is shown in Fig 3. Each individual is therefore described by the number of active terms, the mean error and the standard deviation of the output parameters computed on a reference solution. The dominance rule is applied through these three parameters to evaluate the individual ranking. A fitness value is assigned to the individual based on it's ranking and niching. The error of the new models on a reference solution was evaluated through the following formula:

$$e = 100 \frac{\sum_{i=1}^{N_p} |Q^i - Q_{ref}^i|}{max Q_{ref} \cdot N_p} \tag{16}$$

where Q can be any output parameter (stress/displacement component) and N_p is the number of points along the thickness on which the entity Q is computed. New dominant individuals are selected based on it's fitness. More details about the implementation of genetic algorithms for BTD can be found in Ref. [53]. For the EDZ17 model, 2000 individuals are considered for 200 generations. For the EDZ4 model, 500 individuals for 50 generations are considered. Once the 3D Pareto front is built, the reduced models are

ranked again based on the number of active terms and the objective function $\%Error_{ul}$. As a result, a 2D Pareto front – the BTD - is obtained, as shown in Fig. 4.

6. Results and discussion

A bisinusoidal load was applied to the top surface of the simply supported laminated plate,

$$p = \bar{p}_z \cdot sin\left(\frac{m\pi x}{a}\right) sin\left(\frac{n\pi y}{b}\right) \tag{17}$$

where $a = b = 0.1\ m$, $\bar{p}_z = 1\ kPa$, and m, n = 1. The reduced models were developed considering the displacements u_x, u_y, u_z, and the stresses σ_{xx}, σ_{yy}, σ_{zz}, τ_{xy}, τ_{xz}, and τ_{yz}. The following dimensionless quantities were defined for the displacements and stresses:

$$\bar{u}_x = \frac{u_x \cdot E_2^{k=1} \cdot h^2}{\bar{p}_z \cdot a^3},\ \bar{u}_y = \frac{u_y \cdot E_2^{k=1} \cdot h^2}{\bar{p}_z \cdot a^3},\ \bar{u}_z = \frac{u_z \cdot 100 \cdot E_2^{k=1} \cdot h^3}{\bar{p}_z \cdot a^4},$$

$$\bar{\sigma}_{xx,yy} = \frac{\sigma_{xx,yy}}{\bar{p}_z \cdot (a/h)^2},\ \bar{\sigma}_{zz} = \frac{\sigma_{zz}}{\bar{p}_z},\ \bar{\tau}_{xy} = \frac{\tau_{xy}}{\bar{p}_z \cdot (a/h)^2},\ \bar{\tau}_{xz,yz} = \frac{\tau_{xz,yz}}{\bar{p}_z \cdot (a/h)} \tag{18}$$

where $k = 1$ identifies the bottom layer; $\bar{u}_x$ and $\bar{\tau}_{xz}$ were calculated at $x = 0, y = b/2$; $\bar{u}_y$ and $\bar{\tau}_{yz}$ at $x = a/2, y = 0$; $\bar{u}_z, \bar{\sigma}_{xx}, \bar{\sigma}_{yy}$ and $\bar{\sigma}_{zz}$ at $x = a/2, y = b/2$; $\bar{\tau}_{xy}$ at $x = y = 0$. The shear stresses $\bar{\tau}_{xz}$ and $\bar{\tau}_{yz}$ were computed via the 3D equilibrium equations.

In all the examples considered, the individual laminae were considered of equal thickness and the following set of material properties was used for each lamina: $E_L/E_T = 25$; $G_{LT}/E_T = 0.5$; $G_{TT}/E_T = 0.2$; $\nu_{LT} = \nu_{TT} = 0.25$.

As a reference solution, an LD4 model was considered. The results are reported in Table 4; the three-dimensional exact elasticity results were obtained as in [58, 59]. The LD4 results are in excellent agreement with the reference solution. Consequently, the

LD4 model is used as the reference solution in this paper. Two length-to-thickness ratios were investigated: $^{a}/_{h}$ = 5 and $^{a}/_{h}$ = 20.

6.1 0º/90º/0º

First, to verify the convergence of the GA to the Pareto front, a comparison between the BTDs obtained by the GA and the AAM is presented in Figure 4 for a three-layer, thick plate. The AAM solution was obtained considering all the plate models given by the 2^{18} combinations of terms given by an EDZ4 model, presented in Eq. (3). Each model along the BTD is the one that, for a given errors, requires the minimum number of terms, or, for a given number of terms, provides the best accuracy. The BTDs obtained are in complete agreement. From now on, all the results were obtained using the GA method only.

Figures 5a and 5b compare BTDs built via the EDZ4 and EDZ17 terms. For the sake of clarity, only the lower branch of the BTD is shown, from 24 to six terms. Some of the BTD models given in Fig. 5 are reported in Tables 5 and 6, respectively in which M_E indicates the number of active terms. For instance, the best EDZ17 model with 15 unknown variables for the thick laminated plate ($^{a}/_{h}$ = 5), has the following displacement field:

$$u_x = u_{x_1} + \mathrm{z}u_{x_2} + z^2u_{x_3} + z^3u_{x_4} + (-1)^k\zeta_k u_{x_6} + \sin\left(\frac{\pi z}{h}\right)u_{x_7}$$

$$u_y = u_{y_1} + zu_{y_2} + z^3u_{y_4} + (-1)^k\zeta_k u_{y_6} + \sin\left(\frac{2\pi z}{h}\right)u_{y_8}$$

$$u_z = u_{z_1} + zu_{z_2} + z^2u_{z_3} + z^4u_{z_5} \tag{19}$$

Similarly, the best plate model obtained via EDZ4 with 15 unknown variables is:

$$u_x = u_{x_1} + zu_{x_2} + z^2u_{x_3} + z^3u_{x_4} + (-1)^k\zeta_k u_{x_6}$$

$$u_y = u_{y_1} + \mathrm{z}u_{y_2} + z^2u_{y_3} + z^3u_{y_4} + (-1)^k\zeta_k u_{y_6}$$

$$u_z = u_{z_1} + zu_{z_2} + z^2u_{z_3} + z^3u_{z_4} + z^4u_{z_5} \quad (20)$$

The accuracy of the previous BTD models is given in Tables 7 and 8. For each model, the error on the three displacement and six stress components is given. Also, the mean error, the standard deviation, and $\%Error_{ul}$ are reported. For instance, the plate model of Eq. (19) can detect displacements and stresses with $\%Error_{ul}$ = 0.4302 %, while the plate model of Eq. (20) can detect displacements and stresses with $\%Error_{ul}$ = 0.6112 %. The distribution through the thickness of selected output parameters is shown in Figs. 6 and 7. The EDZ17 reduced models reported in Tables 5 and 6 were used. The refined models are indicated as *hybrid* refined model, N HRM, and *N* is the number of variables in the HRM. The reference solution (LD4) was included for comparison purposes.

The results for the 0º/90º/0º plate suggest that

- The results show that the addition of non-polynomial terms can further enhance the results obtained by the EDZ4 refined models.
- The polynomial terms are essential in the analysis. Concerning the zig-zag terms, the zig-zag term in the u_z displacement field is not needed for both length-to-thickness ratios.
- The trigonometric terms are more effective than the exponential ones.
- The non-polynomial terms are mostly needed in the u_z displacement field, especially in the case with a/h = 20.
- The transverse stress components are those demanding more displacement variables. However, in the thick case, the errors on each displacement and stress

components are quite similar for a given model; that is, all the output variables play an important role in the determination of the active terms.

- The GA approach is a reliable and computationally inexpensive tool to build BTDs. In all cases, the refined best models can detect the 3D-like, LW solution with a considerable lower amount of unknown variables. Some twelve generalized displacement variables are usually enough to meet satisfactory accuracy levels.

6.2 0º/90º

BTDs from EDZ4 and EDZ17 are presented in Fig. 8. Selected BTD models for both length-to-thickness ratios are reported in Tables 9 and 10. For example, the best EDZ17 refined model with fourteen degrees of freedom for $a/h = 20$ is the following:

$$u_x = u_{x_1} + \mathrm{z}u_{x_2} + z^3 u_{x_4} + \sin\left(\frac{2\pi z}{h}\right) u_{x_8}$$

$$u_y = u_{y_1} + \mathrm{z}u_{y_2} + z^3 u_{y_4} + \sin\left(\frac{2\pi z}{h}\right) u_{y_8}$$

$$u_z = u_{z_1} + \mathrm{z}u_{z_2} + z^2 u_{z_3} + z^4 u_{z_5} + (-1)^k \zeta_k u_{z_6} + \cos\left(\frac{2\pi z}{h}\right) u_{z_{12}} \qquad (21)$$

Likewise, the best EDZ4 refined model for the same case is:

$$u_x = u_{x_1} + zu_{x_2} + z^2 u_{x_3} + z^3 u_{x_4}$$

$$u_y = u_{y_1} + \mathrm{z}u_{y_2} + z^2 u_{y_3} + z^3 u_{y_4} + z^4 u_{y_5}$$

$$u_z = u_{z_1} + \mathrm{z}u_{z_2} + z^2 u_{z_3} + z^4 u_{z_5} + (-1)^k \zeta_k u_{z_6} \qquad (22)$$

The refined models considered are compared in Table 11 and 12. Selected displacement and stress distributions along the thickness are presented in Fig. 9 and 10.

The results reported for the 0º/90º case suggest that

- Although the EDZ4 refined models are in good agreements with LD4 results for both length-to-thickness ratios, further improvements can be obtained by adding trigonometric and exponential terms to the plate model. The EDZ17 refined models can obtain better accuracies with less unknown variables.
- All the output variables play a similar role in the determination of the unknown variables. On the other hand, in the moderately thick case, the influence of $\bar{\sigma}_{zz}$ is predominant.
- The polynomial and zig-zag terms are indispensable in the analysis. Regarding the non-polynomial terms, the effectiveness of the exponential and trigonometric terms depends on the length-to-thickness ratio. The former are more important in the thick case, whereas the latter in the moderately thick case.

6.3 0º/90º/90º/0º

BTDs are presented in Fig. 11. Some of the BTDs are shown in in Tables 13 and 14. For instance, the best EDZ17 refined model with ten degrees of freedom for $a/h = 20$ is the following:

$$u_x = zu_{x_2} + z^3 u_{x_4} + \sin\left(\frac{\pi z}{h}\right) u_{x_7}$$

$$u_y = zu_{y_2} + z^3 u_{y_4}$$

$$u_z = u_{z_1} + zu_{z_2} + z^2 u_{z_3} + z^4 u_{z_5} + \cos\left(\frac{2\pi z}{h}\right) u_{z_{12}} \tag{23}$$

Likewise, the best EDZ4 refined model for the same case is:

$$u_x = \mathrm{z}u_{x_2} + z^3 u_{x_4}$$

$$u_y = u_{y_1} + \mathrm{z}u_{y_2} + z^3 u_{y_4}$$

$$u_z = u_{z_1} + z u_{z_2} + z^2 u_{z_3} + z^4 u_{z_5} + (-1)^k \zeta_k u_{z_6} \quad (24)$$

Tables 15 and 16 present the accuracy of the selected plate models, whereas the displacement and stress distributions along the thickness are given in Fig. 12 and 13. The results for the 0º/90º/90º/0º case suggest that

- Important improvements are achieved by employing non-polynomial terms in the plate models. They are particularly noteworthy for thick plates.
- As for the previous case, all the output variables play a significant role in the definition of the displacement field. In the moderately thick case, the transverse axial stress is the most critical component.
- As seen in the previous cases, polynomial terms are indispensable in refined plate models. Concerning the zig-zag terms, only the zig-zag term in the u_z displacement field is needed.
- The exponential terms are more effective than the trigonometric terms for the laminated composite plate studied, especially the exponential terms in the u_x displacement field.

7. Conclusion

Best Theory Diagrams (BTDs) for cross-ply laminated plates considering multiple output parameters have been presented in this paper. The BTD is a curve in which, for a given problem, the most accurate plate models for a given number of unknown variables can be read. In this work, BTDs consider multiple objectives simultaneously; in particular, the three displacement components and the six stress ones. The BTDs are therefore the Pareto fronts of the optimization of the expansions to minimize the error on each displacement and stress component. The axiomatic/asymptotic method together with genetic

algorithms has been employed in the framework of the Carrera Unified Formulation to develop refined ESL plate models. In particular, a combination of Maclaurin, zig-zag, trigonometric and exponential functions has been used to define the displacement field along the thickness of the plate. The results have been presented in terms of displacements and stresses for different length-to-thickness ratios. Simply-supported plates have been analyzed via Navier-type closed form solutions. The following conclusions can be drawn:

(1) Quasi-3D results for multiple output parameters can be obtained by the AAM and the BTD with adequate computational costs. The method presented allows the user to set several output parameters as objective functions in the analysis.
(2) Overall, the addition of trigonometric and exponential terms may improve the accuracy and computational cost of refined plate theories.
(3) Polynomial terms up to the fourth-order are indispensable. The influence of non-polynomial terms is more relevant for thick plates rather than moderately thick ones.
(4) The importance of exponential and trigonometric terms vary depending on the plate configuration. For plates with lamination $0^o/90^o/0^o$, trigonometric terms are more effective than exponential ones. For plates with lamination $0^o/90^o$, exponential and trigonometric terms have different relevance depending on the length-to-thickness ratio.
(5) For plates with lamination $0^o/90^o/90^o/0^o$, exponential terms are more effective than the trigonometric ones.

Future works should tackle the construction of BTDs for dynamic problems.

References

[1] Cauchy AL. Sure l'equilibre et le movement d'une plaque solide. Excercies Matematique 1828;3:328-55.

[2] Poisson SD. Memoire sur l'equilibre et le mouvement des corps elastique. Mem l'Acad Sci 1829;8:357.

[3] Kirchhoff G. Über das Gleichgewicht und die Bewegung einer elastishen Scheibe. J Angew Math 1850; 40: 51-88.

[4] Love AEH The Mathematical Theory of Elasticity, 4th Edition, Cambridge Univ Press, Cambridge, 1927

[5] Reissner E. The effect of transverse shear deformation on the bending of elastic plates. J Appl Mech 1945; 12:69-76.

[6] Mindlin RD. Influence of rotatory inertia and shear in flexural motion of isotropic elastic plates. J Appl Mech 1951; 18: 1031-6.

[7] Rank E, Krause K, Preusch K. On the accuracy of p-version elements for the Reissner-Mindlin plate problem. Int J Numer Methods Eng. 43, 1988; pp. 51-57.

[8] Kant T, Owen DRJ, Zienkiewicz OC. Refined higher order C0 plate bending element. Comput Struct 1982;15:177–83.

[9] Reddy JN. Mechanics of Laminated Plates, Theory and Analysis. CRC Press, Boca Raton, FL, 1997.

[10] Palazotto AN, Dennis ST. Nonlinear analysis of shell structures. AIAA Series; 1992.

[11] M. Touratier. An efficient standard plate theory. International Journal of Engineering Science 1991, 29(8):901 – 916.

[12] Shimpi RP, Ghugal YM. A new layerwise trigonometric shear deformation theory for two-layered cross-ply beams. Compos Sci Technol 2001;61 (9):1271–83.

[13] Arya H, Shimpi RP, Naik NK. A zigzag model for laminated composite beams. Compos Struct 2002;56(1):21–4.

[14] Ferreira AJM, Roque CMC, Jorge RMN. Analysis of composite plates by trigonometric shear deformation theory and multiquadrics. Comp. and Struct. 2005;83(27):2225–37.

[15] Murakami H. Laminated composite plate theory with improved in-plane response. J Appl Mech 1986; 53: 661–6.

[16] E. Carrera, Historical review of zig-zag theories for multilayered plates and shells, Appl. Mech. Rev. 2003, vol. 56, no. 3, pp. 287–308.

[17] E. Reissner, On a mixed variational theorem and on a shear deformable plate theory, Int. J.Numer.Methods Eng. 1986, vol. 23, pp. 193–198.

[18] Librescu L, Reddy JN. A critical review and generalization of transverse shear deformable anisotropic plates. In: Euromech Colloquium 219, Kassel, Refined Dynamical Theories of Beams, Plates and Shells and Their Application, I. Elishakoff and H. Irretier, Ess., Springer-Verlag, Berlin, 1986.

[19] Noor AK, and Burton WS. Assessments of Shear Deformation Theories for Multilayered Composite Plates. Applied Mechanics Reviews. 42, 1989, pp. 1-18.

[20] Noor AK, Burton WS and Bert CW. Computational Model for Sandwich Panels and Shells. Applied Mechanics Reviews. 49, 1996, pp. 155-199.

[21] Kapania K, Raciti S. Recent advances in analysis of laminated beams and plates. Part 1: Shear effects and buckling. AIAA J 1989; 27(7); 923-35.

[22] Reddy JN, Robbins DH. Theories and Computational Models for Composite Laminates. Applied Mechanics Reviews. 47, 1994, pp. 147-165.

[23] Mantari JL, Oktem AS, Guedes Soares C. A new trigonometric shear deformation theory for isotropic, laminated composite and sandwich plates. Int. J. of Sol. and Struct. 2012; 49; pp. 43-53.

[24] Mantari JL, Oktem AS, Guedes Soares C. A new trigonometric layerwise shear deformation theory for the finite element analysis of laminated composite and sandwich plates. Comp. and Struct. 2012; 94-95; pp. 45-53.

[25] Mantari JL, Oktem AS, Guedes Soares C. Bending response of functionally graded plates by using a new higher order shear deformation theory. Composite Structures 2012; 94, pp. 714-723.

[26] Mantari JL, Bonilla EM, Guedes Soares C. A new tangential-exponential higher order shear deformation theory for advanced composite plates. Composites: Part B 2014; 60, pp. 319-328.

[27] Mantari JL, Canales FG. A unified quasi-3D HSDT for the bending analysis of laminated beams. Aerospace Science and Technology 2016; 54, pp. 267-275.

[28] Mantari JL, Canales FG. Free vibration and buckling of laminated beams via hybrid Ritz solution for various penalized boundary conditions. Composite Structures 2016; http://dx.doi.org/10.1016/j.compstruct.2016.05.037.

[29] Mantari JL, Yarasca J. A simple and accurate generalized shear deformation theory for beams. Composite Structures 2015; 134, pp. 593-601.

[30] Yarasca J, Mantari JL, Arciniega RA. Hermite–Lagrangian finite element formulation to study functionally graded sandwich beams. Composite Structures 2016; 140, pp 567-581.

[31] Nguyen TN, Thai CH, Nguyen-Xuan H. On the general framework of high order shear deformation theories for laminated composite plate structures: A novel unified approach. Int. J. of Mech. Sci. 2016; 110; pp. 242-255.

[32] Ramos IA, Mantari JL, Pagani A, Carrera E. Refined theories based on non-polynomial kinematics for the thermoelastic analysis of functionally graded plates, Journal of Thermal Stresses 2016; 39(7):835-853.

[33] Mantari JL, Ramos IA, Carrera E, Petrolo M. Static analysis of functionally graded plates using new non-polynomial displacement fields via Carrera Unified Formulation, Composites Part B 2016; 89:127-142.

[34] Carrera E, Filippi M, Zappino E. Laminated beam analysis by polynomial, trigonometric, exponential and zig-zag theories. European Journal of Mechanics - A/Solids 2013; 41, pp. 58-69.

[35] Carrera E, Filippi M, Zappino E. Free vibration analysis of laminated beam by polynomial, trigonometric, exponential and zig-zag theories. Journal of Composite Materials, Vol. 48, Issue 19, 2014, pp. 2299-2316.

[36] Filippi M, Petrolo M, Valvano S, Carrera E. Analysis of laminated composites and sandwich structures by trigonometric, exponential and miscellaneous polynomials and a MITC9 plate element. Composite Structures 2016; 150, pp. 103-114.

[37] Carrera E, Cinefra M, Li G, Kulikov GM. MITC9 Shell Finite Elements with Miscellaneous Through-the-thickness Functions for the Analysis of Laminated Structures. Composite Structures 2016, doi: http://dx.doi.org/10.1016/j.compstruct.2016.07.032.

[38] Carrera E. Theories and finite elements for multilayered plates and shells: a unified compact formulation with numerical assessment and benchmarking. Arch Comput Meth Eng 2003; 10(3): 215-96.

[39] Carrera E, Brischetto S, Nali P. Plates and shells for smart structures classical and advanced theories for modeling and analysis. Wiley; 2011.

[40] Carrera E, Cinefra M, Petrolo M, Zappino E. Finite Element Analysis of Structures through Unified Formulation. John Wiley & Sons, Inc., Chichester, UK, 2014.

[41] Carrera E, Petrolo M. On the effectiveness of higher-order terms in refined beam theories. Journal of Applied Mechanics 2011; 78. doi: 10.1115/1.4002207.

[42] Carrera E, Petrolo M. Guidelines and recommendation to construct theories for metallic and composite plates. AIAA J. 2012; 48(12): 2852-2866.

[43] Carrera E, Miglioretti F, Petrolo M. Computations and evaluations of higher-order theories for free vibration analysis of beams. Journal of Sound and Vibration 2012; 331:4269-4284. doi: 10.1016/j.jsv.2012.04.017.

[44] Mashat DS, Carrera E, Zenkour AM, Khateeb Al. Axiomatic/asymptotic evaluation of multilayered plate theories by using single and multi-points error criteria. Compos Struct 2013; 106, pp. 393-406.

[45] Mashat DS, Carrera E, Zenkour AM, Khateeb Al. Use of axiomatic/asymptotic approach to evaluate various refined theories for sandwich shells. Compos Struct 2013; 109, pp. 139-149.

[46] Mashat DS, Carrera E, Zenkour AM, Al Katheeb SA, Lamberti A. Evaluation of refined theories for multilayered shells via Axiomatic/Asymptotic method. Journal of Mechanical Science and Technology 2014; 28(11):4663-4672.

[47] Carrera E, Cinefra M, Lamberti A, Petrolo M. Results on best theories for metallic and laminated shells including Layer-Wise models. Composite Structures 2015; 126:285-298.

[48] Petrolo M, Lamberti A. Axiomatic/asymptotic analysis of refined layer-wise theories for composite and sandwich plates. Mech Adv Mater Struct 2016; 23(1): 28-42.

[49] Petrolo M, Cinefra M, Lamberti A, Carrera E. Evaluation of Mixed Theories for Laminated Plates through the Axiomatic/Asymptotic Method. Composites Part B 2015; 76:260-272.

[50] Cinefra M, Lamberti A, Zenkour Ashraf M, Carrera E. Axiomatic/Asymptotic Technique Applied to Refined Theories for Piezoelectric Plates. Mechanics of Advanced Materials and Structures 2015; 22(1-2):107-124.

[51] Carrera E, Cinefra M, Lamberti A, Zenkour AM. Axiomatic/Asymptotic Evaluation of Refined Plate Models for Thermomechanical Analysis. Journal of Thermal Stresses 2015, 38(2), pp. 165-187.

[52] Carrera E, Miglioretti F, Petrolo M. Guidelines and recommendations on the use of higher order finite elements for bending analysis of plates, Int J Comput Methods Eng Sci Mech 2011; 12(6), pp. 303-324.

[53] Carrera E, Miglioretti F. Selection of appropriate multilayered plate theories by using a genetic like algorithm. Composite Structures 2012; 94(3):1175-1186. doi: 10.1016/j.compstruct.2011.10.013.

[54] Petrolo M, Lamberti A, Miglioretti F. Best theory diagram for metallic and laminated composite plates. Mech Adv Mater Struct 2016; 23:9, pp. 1114-1130.

[55] Cinefra M, Carrera E, Lamberti A, Petrolo M. Best Theory Diagrams for multilayered plates considering multifield analysis. Journal of Intelligent Material Systems and Structures In Press.

[56] Deb K. Multi-Objective Optimization using Evolutionary Algorithms. John Wiley & Sons, Inc., Chichester, UK, 2001.

[57] Abdullah Konak, David W Coit, Alice E Smith. Multi-objective optimization using genetic algorithms: A tutorial. Reliability Engineering & System Safety 2006; 91 (9), pp. 992-1007.

[58] Pagano JN, Exact solutions for rectangular bidirectional composites and sandwich plate, J. Compos. Mater., vol. 4, pp. 20–34, 1969.

[59] Pagano JN, Elastic behavior of multilayered bidirectional composites, AIAA J., vol. 10, no. 7, pp. 931–933, 1972.

Tables

Table 1: Expansion terms of the proposed theories.

1	2	3	4	5	6	7	8	9	10
1	z	z^2	z^3	z^4	$(-1)^k\zeta_k$	$sin\left(\frac{\pi z}{h}\right)$	$sin\left(\frac{2\pi z}{h}\right)$	$\sin\left(\frac{3\pi z}{h}\right)$	$\sin\left(\frac{4\pi z}{h}\right)$
1	z	z^2	z^3	z^4	$(-1)^k\zeta_k$	$sin\left(\frac{\pi z}{h}\right)$	$sin\left(\frac{2\pi z}{h}\right)$	$\sin\left(\frac{3\pi z}{h}\right)$	$\sin\left(\frac{4\pi z}{h}\right)$
1	z	z^2	z^3	z^4	$(-1)^k\zeta_k$	$sin\left(\frac{\pi z}{h}\right)$	$sin\left(\frac{2\pi z}{h}\right)$	$\sin\left(\frac{3\pi z}{h}\right)$	$\sin\left(\frac{4\pi z}{h}\right)$

11	12	13	14	15	16	17	18
$\cos\left(\frac{\pi z}{h}\right)$	$\cos\left(\frac{2\pi z}{h}\right)$	$\cos\left(\frac{3\pi z}{h}\right)$	$\cos\left(\frac{4\pi z}{h}\right)$	$e^{\frac{z}{h}}$	$e^{\frac{2z}{h}}$	$e^{\frac{3z}{h}}$	$e^{\frac{4z}{h}}$
$\cos\left(\frac{\pi z}{h}\right)$	$\cos\left(\frac{2\pi z}{h}\right)$	$\cos\left(\frac{3\pi z}{h}\right)$	$\cos\left(\frac{4\pi z}{h}\right)$	$e^{\frac{z}{h}}$	$e^{\frac{2z}{h}}$	$e^{\frac{3z}{h}}$	$e^{\frac{4z}{h}}$
$\cos\left(\frac{\pi z}{h}\right)$	$\cos\left(\frac{2\pi z}{h}\right)$	$\cos\left(\frac{3\pi z}{h}\right)$	$\cos\left(\frac{4\pi z}{h}\right)$	$e^{\frac{z}{h}}$	$e^{\frac{2z}{h}}$	$e^{\frac{3z}{h}}$	$e^{\frac{4z}{h}}$

Table 2: Example of model representation.

Full model representation					Reduced model representation				
▲	▲	▲	▲	▲	▲	Δ	▲	▲	▲
▲	▲	▲	▲	▲	▲	▲	▲	▲	▲
▲	▲	▲	▲	▲	▲	▲	▲	▲	▲

Table 3: Symbols to indicate the status of a displacement variable.

Active term	Inactive terms
▲	Δ

Table 4: LD4 model assessment for 3-layer and 5-layer laminated plates.

	$\bar{\sigma}_{xx}(z=\pm h/2)$		$\bar{\sigma}_{yy}(z=\pm h/6)$		$\bar{\tau}_{xz}(z=0)$	$\bar{\tau}_{yz}(z=0)$	$\bar{\tau}_{xy}(z=\pm h/2)$	
				$a/h = 100$				
				3-layer laminate (0º/90º/0º)				
Ref. [58]	±0.539		±0.181		0.395	0.0828	±0.0213	
LD4	±0.539		±0.1808		0.3946	0.0828	±0.0213	
				5-layer laminate (0º/90º/0º/90º/0º)				
	$\bar{\sigma}_{xx}(z=\pm h/2)$		$\bar{\sigma}_{yy}(z=\pm h/3)$		$\bar{\tau}_{xz}(z=0)$	$\bar{\tau}_{yz}(z=0)$	$\bar{\tau}_{xy}(z=\pm h/2)$	
Ref. [59]	±0.539		±0.360		0.272	0.205	±0.0213	
LD4	±0.5386		±0.3600		0.2720	0.2055	±0.0213	
				$a/h = 4$				
				3-layer laminate (0º/90º/0º)				
	$\bar{\sigma}_{xx}(z=\pm h/2)$		$\bar{\sigma}_{yy}(z=\pm h/6)$		$\bar{\tau}_{xz}(z=0)$	$\bar{\tau}_{yz}(z=0)$	$\bar{\tau}_{xy}(z=\pm h/2)$	
Ref. [58]	0.801	-0.755	0.534	-0.556	0.256	0.2172	-0.0511	0.0505
LD4	0.8008	-0.7547	0.5341	-0.5562	0.2559	0.2179	-0.0510	0.0505
				5-layer laminate (0º/90º/0º/90º/0º)				
	$\bar{\sigma}_{xx}(z=\pm h/2)$		$\bar{\sigma}_{yy}(z=\pm h/3)$		$\bar{\tau}_{xz}(z=0)$	$\bar{\tau}_{yz}(z=0)$	$\bar{\tau}_{xy}(z=\pm h/2)$	
Ref. [59]	0.685	-0.651	0.633	-0.626	0.238	0.229	-0.0394	0.0384
LD4	0.6852	-0.6512	0.6334	-0.6256	0.2378	0.2289	-0.0393	0.0384

Table 5: Best EDZ17 models, 0º/90º/0º, $^{a}/_{h} = 5$.

$M_E = {}^{7}/_{54}$, $\%Error_{ul}$ = 3.3590

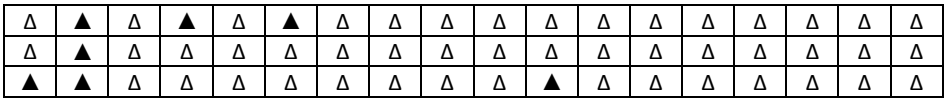

$M_E = {}^{9}/_{54}$, $\%Error_{ul}$ = 2.2010

$M_E = {}^{12}/_{54}$, $\%Error_{ul}$ = 0.6713

$M_E = {}^{15}/_{54}$, $\%Error_{ul}$ = 0.4302

$M_E = {}^{18}/_{54}$, $\%Error_{ul}$ = 0.2900

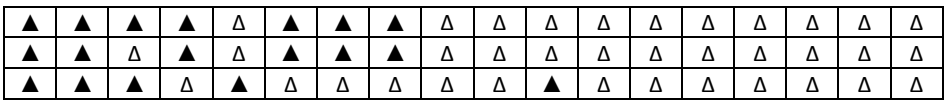

$M_E = {}^{21}/_{54}$, $\%Error_{ul}$ = 0.2475

Table 6: Best EDZ17 models, 0º/90º/0º, $^{a}/_{h} = 20$.

$M_E = {}^{7}/_{54}$, $\%Error_{ul}$ = 1.6493

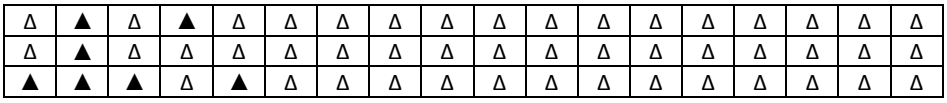

$M_E = {}^{9}/_{54}$, $\%Error_{ul}$ = 0.5888

$M_E = {}^{12}/_{54}$, $\%Error_{ul}$ = 0.3979

$M_E = {}^{15}/_{54}$, $\%Error_{ul}$ = 0.3160

$M_E = {}^{19}/_{54}$, $\%Error_{ul}$ = 0.2678

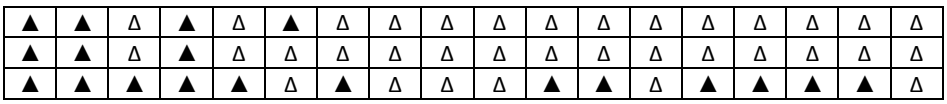

$M_E = {}^{21}/_{54}$, $\%Error_{ul}$ = 0.2498

Table 7: Comparison between the accuracies of best EDZ4 and EDZ17 models in computing displacement and stress components, 0º/90º/0º, $^{a}/_{h} = 5$.

	$M_E = {}^{7}/_{54}$, μ = 2.1125, σ = 1.2465, $\%Error_{ul}$ = 3.3590								
	e (%)								
	$\bar{u}_x$	$\bar{u}_y$	$\bar{u}_z$	$\bar{\sigma}_{xx}$	$\bar{\sigma}_{yy}$	$\bar{\tau}_{xy}$	$\bar{\tau}_{xz}$	$\bar{\tau}_{yz}$	$\bar{\sigma}_{zz}$
EDZ17	1.732	1.460	0.839	0.826	1.381	1.285	3.645	3.787	4.053
EDZ4	3.128	1.571	3.285	2.120	1.172	1.787	3.000	4.541	3.248
	$M_E = {}^{9}/_{54}$, μ = 1.4259, σ = 0.7750, $\%Error_{ul}$ = 2.2010								
	e (%)								
	$\bar{u}_x$	$\bar{u}_y$	$\bar{u}_z$	$\bar{\sigma}_{xx}$	$\bar{\sigma}_{yy}$	$\bar{\tau}_{xy}$	$\bar{\tau}_{xz}$	$\bar{\tau}_{yz}$	$\bar{\sigma}_{zz}$
EDZ17	1.726	1.362	0.914	0.816	1.224	0.903	3.468	0.988	1.428
EDZ4	1.184	1.435	0.914	0.668	1.363	1.021	0.901	3.566	1.428
	$M_E = {}^{12}/_{54}$, μ = 0.4888, σ = 0.1824, $\%Error_{ul}$ = 0.6713								
	e (%)								
	$\bar{u}_x$	$\bar{u}_y$	$\bar{u}_z$	$\bar{\sigma}_{xx}$	$\bar{\sigma}_{yy}$	$\bar{\tau}_{xy}$	$\bar{\tau}_{xz}$	$\bar{\tau}_{yz}$	$\bar{\sigma}_{zz}$
EDZ17	0.603	0.481	0.388	0.478	0.446	0.390	0.460	0.223	0.928
EDZ4	0.603	0.481	0.388	0.478	0.446	0.390	0.460	0.223	0.928
	$M_E = {}^{15}/_{54}$, μ = 0.2459, σ = 0.1843, $\%Error_{ul}$ = 0.4302								
	e (%)								
	$\bar{u}_x$	$\bar{u}_y$	$\bar{u}_z$	$\bar{\sigma}_{xx}$	$\bar{\sigma}_{yy}$	$\bar{\tau}_{xy}$	$\bar{\tau}_{xz}$	$\bar{\tau}_{yz}$	$\bar{\sigma}_{zz}$
EDZ17	0.229	0.291	0.078	0.065	0.235	0.242	0.131	0.214	0.723
EDZ4	0.606	0.476	0.317	0.484	0.517	0.358	0.449	0.361	0.759
	$M_E = {}^{18}/_{54}$, μ = 0.1398, σ = 0.1502, $\%Error_{ul}$ = 0.2900								
	e (%)								
	$\bar{u}_x$	$\bar{u}_y$	$\bar{u}_z$	$\bar{\sigma}_{xx}$	$\bar{\sigma}_{yy}$	$\bar{\tau}_{xy}$	$\bar{\tau}_{xz}$	$\bar{\tau}_{yz}$	$\bar{\sigma}_{zz}$
EDZ17	0.135	0.125	0.011	0.050	0.061	0.107	0.101	0.112	0.550
EDZ4	0.598	0.475	0.317	0.484	0.514	0.343	0.449	0.361	0.758
	$M_E = {}^{21}/_{54}$, μ = 0.1153, σ = 0.1321, $\%Error_{ul}$ = 0.2475								
	e (%)								
	$\bar{u}_x$	$\bar{u}_y$	$\bar{u}_z$	$\bar{\sigma}_{xx}$	$\bar{\sigma}_{yy}$	$\bar{\tau}_{xy}$	$\bar{\tau}_{xz}$	$\bar{\tau}_{yz}$	$\bar{\sigma}_{zz}$
EDZ17	0.132	0.051	0.010	0.051	0.057	0.061	0.101	0.094	0.477

Table 8: Comparison between the accuracies of best EDZ4 and EDZ17 models in computing displacement and stress components, 0º/90º/0º, $^{a}/_{h} = 20$.

	$M_E = {}^{7}/_{54}$, μ = 1.0443, σ = 0.6049, $\%Error_{ul}$ = 1.6493								
	e (%)								
	$\bar{u}_x$	$\bar{u}_y$	$\bar{u}_z$	$\bar{\sigma}_{xx}$	$\bar{\sigma}_{yy}$	$\bar{\tau}_{xy}$	$\bar{\tau}_{xz}$	$\bar{\tau}_{yz}$	$\bar{\sigma}_{zz}$
EDZ17	1.056	0.996	2.176	0.601	0.405	0.688	0.380	1.140	1.954
EDZ4	1.056	0.996	2.176	0.601	0.405	0.688	0.380	1.140	1.954
	$M_E = {}^{9}/_{54}$, μ = 0.2640, σ = 0.3247, $\%Error_{ul}$ = 0.5888								
	e (%)								
	$\bar{u}_x$	$\bar{u}_y$	$\bar{u}_z$	$\bar{\sigma}_{xx}$	$\bar{\sigma}_{yy}$	$\bar{\tau}_{xy}$	$\bar{\tau}_{xz}$	$\bar{\tau}_{yz}$	$\bar{\sigma}_{zz}$
EDZ17	0.092	0.149	0.033	0.061	0.149	0.115	0.169	0.496	1.109
EDZ4	0.092	0.115	0.033	0.059	0.094	0.059	0.158	0.077	1.301
	$M_E = {}^{12}/_{54}$, μ = 0.1668, σ = 0.2311, $\%Error_{ul}$ = 0.3979								
	e (%)								
	$\bar{u}_x$	$\bar{u}_y$	$\bar{u}_z$	$\bar{\sigma}_{xx}$	$\bar{\sigma}_{yy}$	$\bar{\tau}_{xy}$	$\bar{\tau}_{xz}$	$\bar{\tau}_{yz}$	$\bar{\sigma}_{zz}$
EDZ17	0.092	0.115	0.033	0.059	0.092	0.059	0.158	0.077	0.813
EDZ4	0.027	0.115	0.033	0.014	0.093	0.052	0.019	0.077	1.298
	$M_E = {}^{15}/_{54}$, μ = 0.0985, σ = 0.2174, $\%Error_{ul}$ = 0.3160								
	e (%)								
	$\bar{u}_x$	$\bar{u}_y$	$\bar{u}_z$	$\bar{\sigma}_{xx}$	$\bar{\sigma}_{yy}$	$\bar{\tau}_{xy}$	$\bar{\tau}_{xz}$	$\bar{\tau}_{yz}$	$\bar{\sigma}_{zz}$
EDZ17	0.018	0.051	0.012	0.006	0.031	0.026	0.006	0.021	0.712
	$M_E = {}^{19}/_{54}$, μ = 0.0859, σ = 0.1818, $\%Error_{ul}$ = 0.2678								
	e (%)								
	$\bar{u}_x$	$\bar{u}_y$	$\bar{u}_z$	$\bar{\sigma}_{xx}$	$\bar{\sigma}_{yy}$	$\bar{\tau}_{xy}$	$\bar{\tau}_{xz}$	$\bar{\tau}_{yz}$	$\bar{\sigma}_{zz}$
EDZ17	0.018	0.051	0.012	0.006	0.031	0.026	0.006	0.021	0.599
	$M_E = {}^{21}/_{54}$, μ = 0.0736, σ = 0.1762, $\%Error_{ul}$ = 0.2498								
	e (%)								
	$\bar{u}_x$	$\bar{u}_y$	$\bar{u}_z$	$\bar{\sigma}_{xx}$	$\bar{\sigma}_{yy}$	$\bar{\tau}_{xy}$	$\bar{\tau}_{xz}$	$\bar{\tau}_{yz}$	$\bar{\sigma}_{zz}$
EDZ17	0.016	0.019	0.004	0.005	0.017	0.009	0.004	0.013	0.571

Table 9: Best EDZ17 models, 0º/90º, $^{a}/_{h} = 5$.

$M_E = {}^{7}/_{54}$, $\%Error_{ul}$ = 3.1976

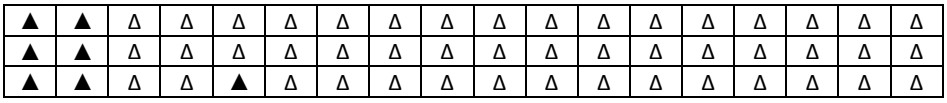

$M_E = {}^{9}/_{54}$, $\%Error_{ul}$ = 1.9212

$M_E = {}^{12}/_{54}$, $\%Error_{ul}$ = 0.8463

$M_E = {}^{15}/_{54}$, $\%Error_{ul}$ = 0.6863

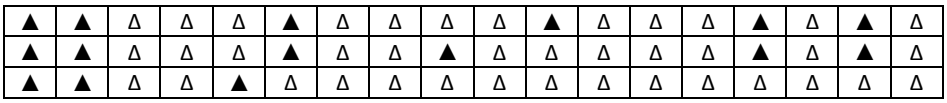

$M_E = {}^{18}/_{54}$, $\%Error_{ul}$ = 0.4524

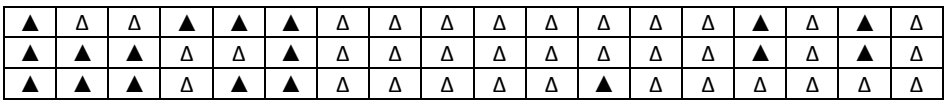

$M_E = {}^{21}/_{54}$, $\%Error_{ul}$ = 0.2791

Table 10: Best EDZ17 models, 0º/90º, $^{a}/_{h} = 20$.

$M_E = {}^{8}/_{54}$, $\%Error_{ul}$ = 1.3690

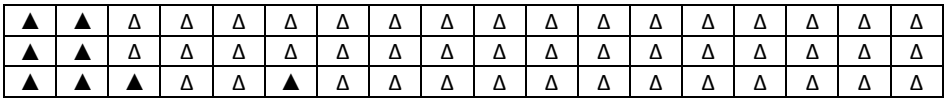

$M_E = {}^{11}/_{54}$, $\%Error_{ul}$ = 0.7074

$M_E = {}^{14}/_{54}$, $\%Error_{ul}$ = 0.1415

$M_E = {}^{18}/_{54}$, $\%Error_{ul}$ = 0.0633

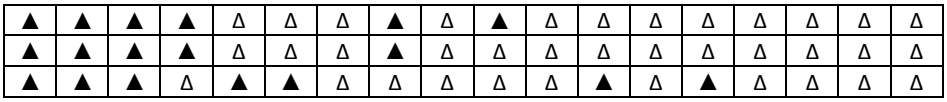

$M_E = {}^{21}/_{54}$, $\%Error_{ul}$ = 0.0397

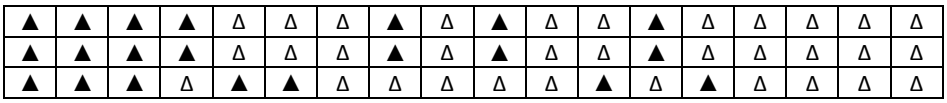

Table 11: Comparison between the accuracies of best EDZ4 and EDZ17 models in computing displacement and stress components, 0º/90º, $^{a}/_{h} = 5$.

	$M_E = {}^{7}/_{54}$, μ = 2.0630, σ = 1.1346, $\%Error_{ul}$ = 3.1976								
	e (%)								
	$\bar{u}_x$	$\bar{u}_y$	$\bar{u}_z$	$\bar{\sigma}_{xx}$	$\bar{\sigma}_{yy}$	$\bar{\tau}_{xy}$	$\bar{\tau}_{xz}$	$\bar{\tau}_{yz}$	$\bar{\sigma}_{zz}$
EDZ17	1.814	1.559	5.003	1.695	1.653	1.690	1.239	1.094	2.815
EDZ4	1.814	1.559	5.003	1.695	1.653	1.690	1.239	1.094	2.815
	$M_E = {}^{9}/_{54}$, μ = 1.2676, σ = 0.6536, $\%Error_{ul}$ = 1.9212								
	e (%)								
	$\bar{u}_x$	$\bar{u}_y$	$\bar{u}_z$	$\bar{\sigma}_{xx}$	$\bar{\sigma}_{yy}$	$\bar{\tau}_{xy}$	$\bar{\tau}_{xz}$	$\bar{\tau}_{yz}$	$\bar{\sigma}_{zz}$
EDZ17	1.077	0.740	2.454	1.512	0.730	0.988	0.945	0.612	2.346
EDZ4	1.533	1.591	3.379	1.177	1.773	1.573	0.899	1.392	1.827
	$M_E = {}^{12}/_{54}$, μ = 0.6455, σ = 0.2007, $\%Error_{ul}$ = 0.8463								
	e (%)								
	$\bar{u}_x$	$\bar{u}_y$	$\bar{u}_z$	$\bar{\sigma}_{xx}$	$\bar{\sigma}_{yy}$	$\bar{\tau}_{xy}$	$\bar{\tau}_{xz}$	$\bar{\tau}_{yz}$	$\bar{\sigma}_{zz}$
EDZ17	0.603	0.481	0.388	0.478	0.446	0.390	0.460	0.223	0.928
EDZ4	1.017	0.812	1.650	1.168	0.872	0.972	0.801	0.504	0.984
	$M_E = {}^{15}/_{54}$, μ = 0.3998, σ = 0.2865, $\%Error_{ul}$ = 0.6863								
	e (%)								
	$\bar{u}_x$	$\bar{u}_y$	$\bar{u}_z$	$\bar{\sigma}_{xx}$	$\bar{\sigma}_{yy}$	$\bar{\tau}_{xy}$	$\bar{\tau}_{xz}$	$\bar{\tau}_{yz}$	$\bar{\sigma}_{zz}$
EDZ17	0.346	0.312	0.223	0.203	0.187	0.457	0.370	0.320	1.176
EDZ4	0.648	0.687	0.518	0.384	0.405	0.895	0.432	0.459	0.982
	$M_E = {}^{18}/_{54}$, μ = 0.3740, σ = 0.0784, $\%Error_{ul}$ = 0.4524								
	e (%)								
	$\bar{u}_x$	$\bar{u}_y$	$\bar{u}_z$	$\bar{\sigma}_{xx}$	$\bar{\sigma}_{yy}$	$\bar{\tau}_{xy}$	$\bar{\tau}_{xz}$	$\bar{\tau}_{yz}$	$\bar{\sigma}_{zz}$
EDZ17	0.377	0.420	0.245	0.235	0.382	0.464	0.395	0.375	0.467
	$M_E = {}^{21}/_{54}$, μ = 0.1847, σ = 0.0944, $\%Error_{ul}$ = 0.2791								
	e (%)								
	$\bar{u}_x$	$\bar{u}_y$	$\bar{u}_z$	$\bar{\sigma}_{xx}$	$\bar{\sigma}_{yy}$	$\bar{\tau}_{xy}$	$\bar{\tau}_{xz}$	$\bar{\tau}_{yz}$	$\bar{\sigma}_{zz}$
EDZ17	0.132	0.124	0.067	0.094	0.171	0.158	0.315	0.361	0.236

Table 12: Comparison between the accuracies of best EDZ4 and EDZ17 models in computing displacement and stress components, 0º/90º, $^{a}/_{h} = 20$.

	$M_E = {}^{8}/_{54}$, μ = 0.4753, σ = 0.8936, $\%Error_{ul}$ = 1.3690								
	e (%)								
	$\bar{u}_x$	$\bar{u}_y$	$\bar{u}_z$	$\bar{\sigma}_{xx}$	$\bar{\sigma}_{yy}$	$\bar{\tau}_{xy}$	$\bar{\tau}_{xz}$	$\bar{\tau}_{yz}$	$\bar{\sigma}_{zz}$
EDZ17	0.127	0.126	0.504	0.122	0.122	0.120	0.088	0.087	2.979
EDZ4	0.127	0.126	0.504	0.122	0.122	0.120	0.088	0.087	2.979
	$M_E = {}^{11}/_{54}$, μ = 0.3123, σ = 0.3951, $\%Error_{ul}$ = 0.7074								
	e (%)								
	$\bar{u}_x$	$\bar{u}_y$	$\bar{u}_z$	$\bar{\sigma}_{xx}$	$\bar{\sigma}_{yy}$	$\bar{\tau}_{xy}$	$\bar{\tau}_{xz}$	$\bar{\tau}_{yz}$	$\bar{\sigma}_{zz}$
EDZ17	0.190	0.189	0.266	0.131	0.129	0.218	0.132	0.130	1.422
EDZ4	0.190	0.189	0.266	0.131	0.129	0.218	0.132	0.130	1.422
	$M_E = {}^{14}/_{54}$, μ = 0.1057, σ = 0.0358, $\%Error_{ul}$ = 0.1415								
	e (%)								
	$\bar{u}_x$	$\bar{u}_y$	$\bar{u}_z$	$\bar{\sigma}_{xx}$	$\bar{\sigma}_{yy}$	$\bar{\tau}_{xy}$	$\bar{\tau}_{xz}$	$\bar{\tau}_{yz}$	$\bar{\sigma}_{zz}$
EDZ17	0.115	0.114	0.132	0.067	0.066	0.113	0.079	0.078	0.184
EDZ4	0.093	0.055	0.169	0.090	0.059	0.088	0.069	0.032	1.390
	$M_E = {}^{18}/_{54}$, μ = 0.0399, σ = 0.0234, $\%Error_{ul}$ = 0.0633								
	e (%)								
	$\bar{u}_x$	$\bar{u}_y$	$\bar{u}_z$	$\bar{\sigma}_{xx}$	$\bar{\sigma}_{yy}$	$\bar{\tau}_{xy}$	$\bar{\tau}_{xz}$	$\bar{\tau}_{yz}$	$\bar{\sigma}_{zz}$
EDZ17	0.036	0.036	0.064	0.024	0.024	0.033	0.020	0.024	0.096
	$M_E = {}^{21}/_{54}$, μ = 0.0250, σ = 0.0147, $\%Error_{ul}$ = 0.0397								
	e (%)								
	$\bar{u}_x$	$\bar{u}_y$	$\bar{u}_z$	$\bar{\sigma}_{xx}$	$\bar{\sigma}_{yy}$	$\bar{\tau}_{xy}$	$\bar{\tau}_{xz}$	$\bar{\tau}_{yz}$	$\bar{\sigma}_{zz}$
EDZ17	0.019	0.019	0.039	0.011	0.011	0.018	0.022	0.022	0.060

Table 13: Best EDZ17 models, 0º/90º/90º/0º, $^{a}/_{h} = 5$.

$M_E = {}^{9}/_{54}$, $\%Error_{ul}$ = 3.2985

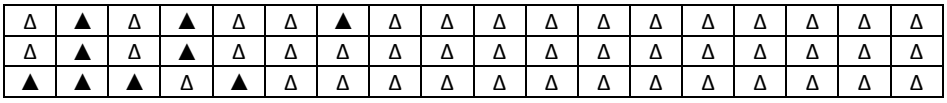

$M_E = {}^{12}/_{54}$, $\%Error_{ul}$ = 2.0088

$M_E = {}^{15}/_{54}$, $\%Error_{ul}$ = 1.4414

$M_E = {}^{18}/_{54}$, $\%Error_{ul}$ = 1.1586

$M_E = {}^{21}/_{54}$, $\%Error_{ul}$ = 0.8212

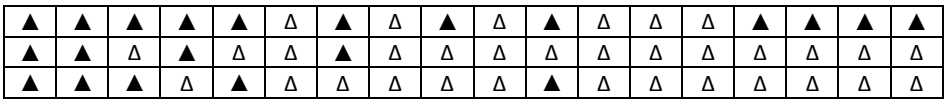

Table 14: Best EDZ17 models, 0º/90º/90º/0º, $^{a}/_{h} = 20$.

$M_E = {}^{7}/_{54}$, $\%Error_{ul}$ = 1.2881

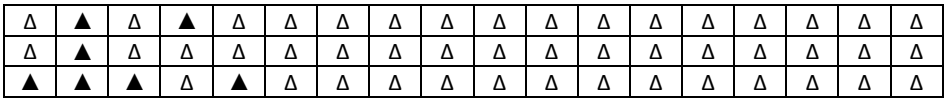

$M_E = {}^{10}/_{54}$, $\%Error_{ul}$ = 0.7098

$M_E = {}^{13}/_{54}$, $\%Error_{ul}$ = 0.5242

$M_E = {}^{16}/_{54}$, $\%Error_{ul}$ = 0.4327

$M_E = {}^{20}/_{54}$, $\%Error_{ul}$ = 0.3199

Table 15: Comparison between the accuracies of best EDZ4 and EDZ17 models in computing displacement and stress components, 0º/90º/90º/0º, $^{a}/_{h} = 5$.

	$M_E = {}^{9}/_{54}$, μ = 2.2857, σ = 1.0127, $\%Error_{ul}$ = 3.2985								
	e (%)								
	$\bar{u}_x$	$\bar{u}_y$	$\bar{u}_z$	$\bar{\sigma}_{xx}$	$\bar{\sigma}_{yy}$	$\bar{\tau}_{xy}$	$\bar{\tau}_{xz}$	$\bar{\tau}_{yz}$	$\bar{\sigma}_{zz}$
EDZ17	3.974	1.887	2.570	1.356	1.173	1.838	3.127	3.571	1.071
EDZ4	4.857	2.109	3.390	1.897	0.981	2.075	2.593	0.652	1.268
	$M_E = {}^{12}/_{54}$, μ = 1.3057, σ = 0.7030, $\%Error_{ul}$ = 2.0088								
	e (%)								
	$\bar{u}_x$	$\bar{u}_y$	$\bar{u}_z$	$\bar{\sigma}_{xx}$	$\bar{\sigma}_{yy}$	$\bar{\tau}_{xy}$	$\bar{\tau}_{xz}$	$\bar{\tau}_{yz}$	$\bar{\sigma}_{zz}$
EDZ17	2.788	1.648	2.119	0.764	0.988	1.218	1.004	0.549	0.669
EDZ4	3.785	2.110	3.390	1.792	0.984	1.863	1.892	0.652	1.025
	$M_E = {}^{15}/_{54}$, μ = 0.9034, σ = 0.5379, $\%Error_{ul}$ = 1.4414								
	e (%)								
	$\bar{u}_x$	$\bar{u}_y$	$\bar{u}_z$	$\bar{\sigma}_{xx}$	$\bar{\sigma}_{yy}$	$\bar{\tau}_{xy}$	$\bar{\tau}_{xz}$	$\bar{\tau}_{yz}$	$\bar{\sigma}_{zz}$
EDZ17	2.179	0.464	1.436	0.658	0.425	0.719	0.958	0.503	0.784
EDZ4	3.776	2.108	3.390	1.793	0.978	1.860	1.892	0.651	1.018
	$M_E = {}^{18}/_{54}$, μ = 0.7391, σ = 0.4194, $\%Error_{ul}$ = 1.1586								
	e (%)								
	$\bar{u}_x$	$\bar{u}_y$	$\bar{u}_z$	$\bar{\sigma}_{xx}$	$\bar{\sigma}_{yy}$	$\bar{\tau}_{xy}$	$\bar{\tau}_{xz}$	$\bar{\tau}_{yz}$	$\bar{\sigma}_{zz}$
EDZ17	1.662	0.432	1.305	0.510	0.391	0.566	0.553	0.459	0.771
	$M_E = {}^{21}/_{54}$, μ = 0.5425, σ = 0.2786, $\%Error_{ul}$ = 0.8212								
	e (%)								
	$\bar{u}_x$	$\bar{u}_y$	$\bar{u}_z$	$\bar{\sigma}_{xx}$	$\bar{\sigma}_{yy}$	$\bar{\tau}_{xy}$	$\bar{\tau}_{xz}$	$\bar{\tau}_{yz}$	$\bar{\sigma}_{zz}$
EDZ17	1.099	0.370	0.982	0.369	0.311	0.415	0.395	0.339	0.599

Table 16: Comparison between the accuracies of best EDZ4 and EDZ17 models in computing displacement and stress components, 0º/90º/90º/0º, $^{a}/_{h} = 20$.

	$M_E = {}^{7}/_{54}$, μ = 0.6530, σ = 0.6351, $\%Error_{ul}$ = 1.2881								
	e (%)								
	$\bar{u}_x$	$\bar{u}_y$	$\bar{u}_z$	$\bar{\sigma}_{xx}$	$\bar{\sigma}_{yy}$	$\bar{\tau}_{xy}$	$\bar{\tau}_{xz}$	$\bar{\tau}_{yz}$	$\bar{\sigma}_{zz}$
EDZ17	0.490	0.510	1.199	0.240	0.155	0.396	0.150	0.493	2.241
EDZ4	0.127	0.126	0.504	0.122	0.122	0.120	0.088	0.087	2.979
	$M_E = {}^{10}/_{54}$, μ = 0.4298, σ = 0.2800, $\%Error_{ul}$ = 0.7098								
	e (%)								
	$\bar{u}_x$	$\bar{u}_y$	$\bar{u}_z$	$\bar{\sigma}_{xx}$	$\bar{\sigma}_{yy}$	$\bar{\tau}_{xy}$	$\bar{\tau}_{xz}$	$\bar{\tau}_{yz}$	$\bar{\sigma}_{zz}$
EDZ17	0.395	0.400	0.797	0.173	0.183	0.257	0.117	0.570	0.973
EDZ4	0.190	0.189	0.266	0.131	0.129	0.218	0.132	0.130	1.422
	$M_E = {}^{13}/_{54}$, μ = 0.3182, σ = 0.2060, $\%Error_{ul}$ = 0.5242								
	e (%)								
	$\bar{u}_x$	$\bar{u}_y$	$\bar{u}_z$	$\bar{\sigma}_{xx}$	$\bar{\sigma}_{yy}$	$\bar{\tau}_{xy}$	$\bar{\tau}_{xz}$	$\bar{\tau}_{yz}$	$\bar{\sigma}_{zz}$
EDZ17	0.276	0.300	0.571	0.083	0.146	0.193	0.116	0.464	0.710
EDZ4	0.093	0.055	0.169	0.090	0.059	0.088	0.069	0.032	1.390
	$M_E = {}^{16}/_{54}$, μ = 0.2584, σ = 0.1742, $\%Error_{ul}$ = 0.4327								
	e (%)								
	$\bar{u}_x$	$\bar{u}_y$	$\bar{u}_z$	$\bar{\sigma}_{xx}$	$\bar{\sigma}_{yy}$	$\bar{\tau}_{xy}$	$\bar{\tau}_{xz}$	$\bar{\tau}_{yz}$	$\bar{\sigma}_{zz}$
EDZ17	0.281	0.266	0.558	0.083	0.087	0.194	0.158	0.132	0.562
	$M_E = {}^{20}/_{54}$, μ = 0.1975, σ = 0.1223, $\%Error_{ul}$ = 0.3199								
	e (%)								
	$\bar{u}_x$	$\bar{u}_y$	$\bar{u}_z$	$\bar{\sigma}_{xx}$	$\bar{\sigma}_{yy}$	$\bar{\tau}_{xy}$	$\bar{\tau}_{xz}$	$\bar{\tau}_{yz}$	$\bar{\sigma}_{zz}$
EDZ17	0.188	0.186	0.418	0.082	0.115	0.113	0.115	0.140	0.418

Figures

Figure 1. Plate geometry and reference system.

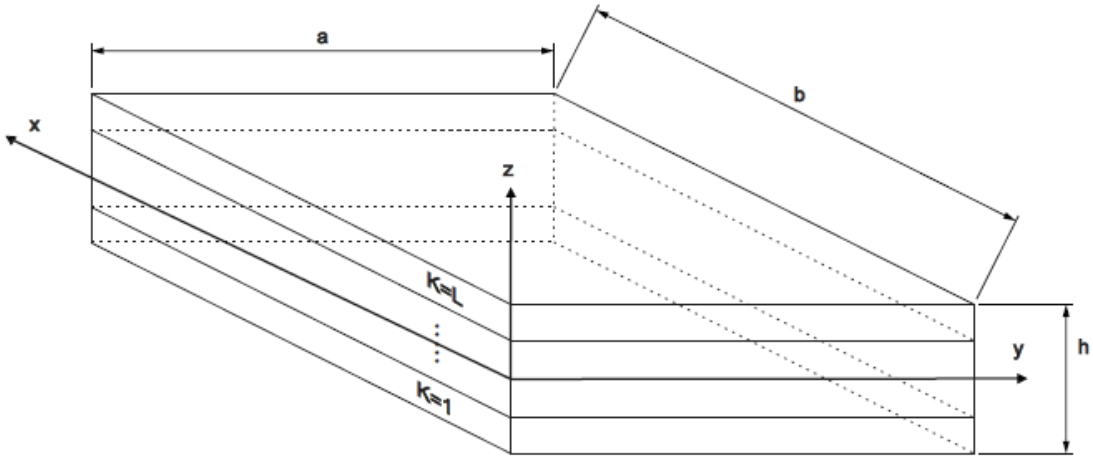

Figure 2. 3D Pareto front via AAM, EDZ4, 0º/90º/0º, $^{a}/_{h}$ = 5.

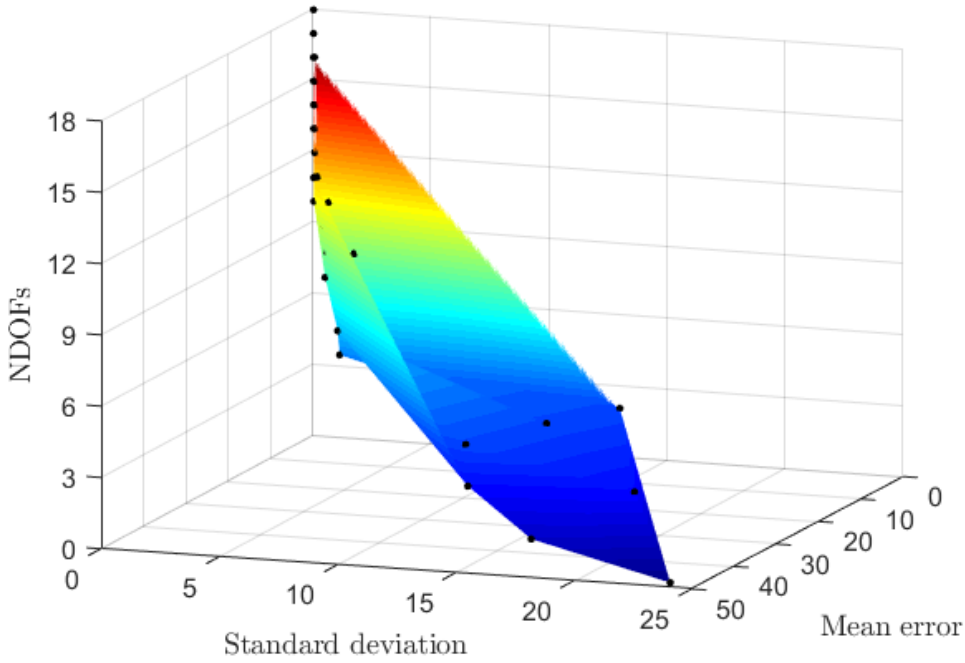

Figure 3. Displacement field of a refined model and genes of a chromosome.

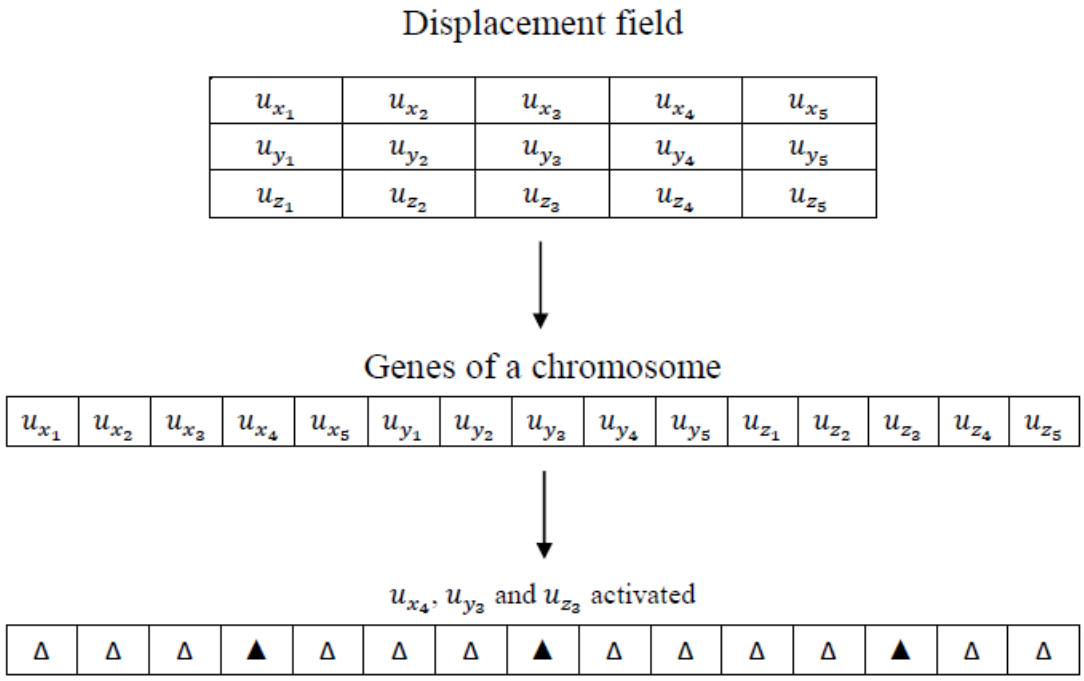

Figure 4. BTD based on EDZ4 via GA and AAM, 0º/90º/0º, $^{a}/_{h}$ = 5.

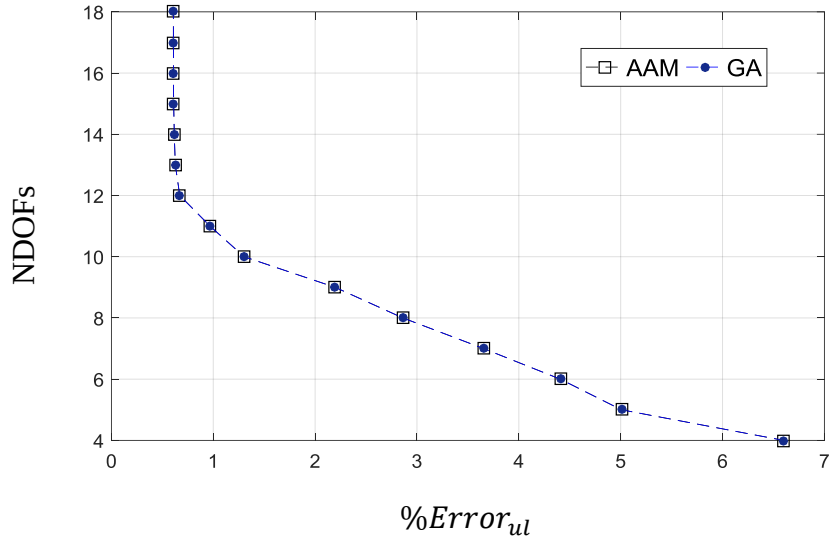

Figure 5. BTDs for 0º/90º/0º, (a) $^{a}/_{h}$ = 5, (b) $^{a}/_{h}$ = 20.

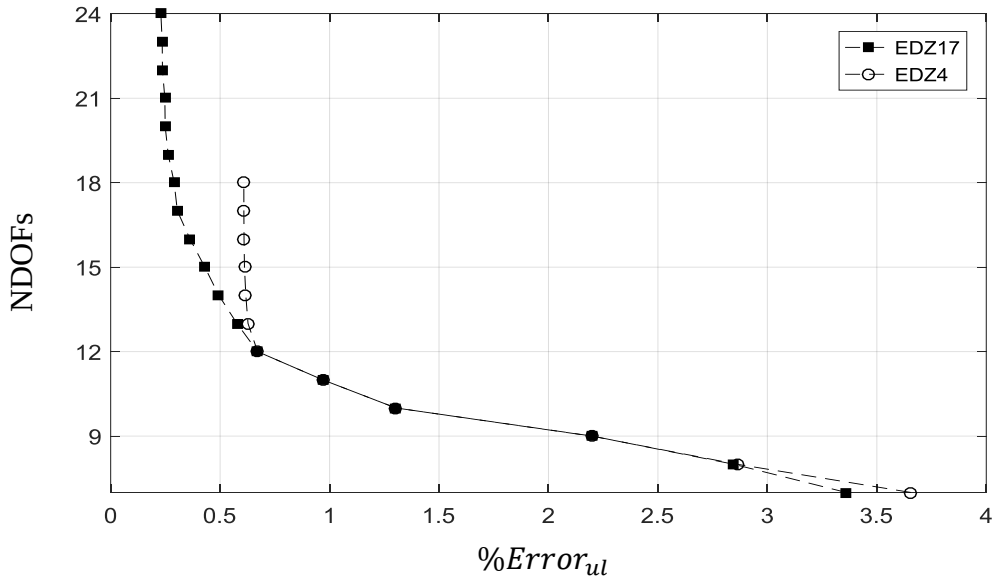

(a) $^{a}/_{h}$ = 5

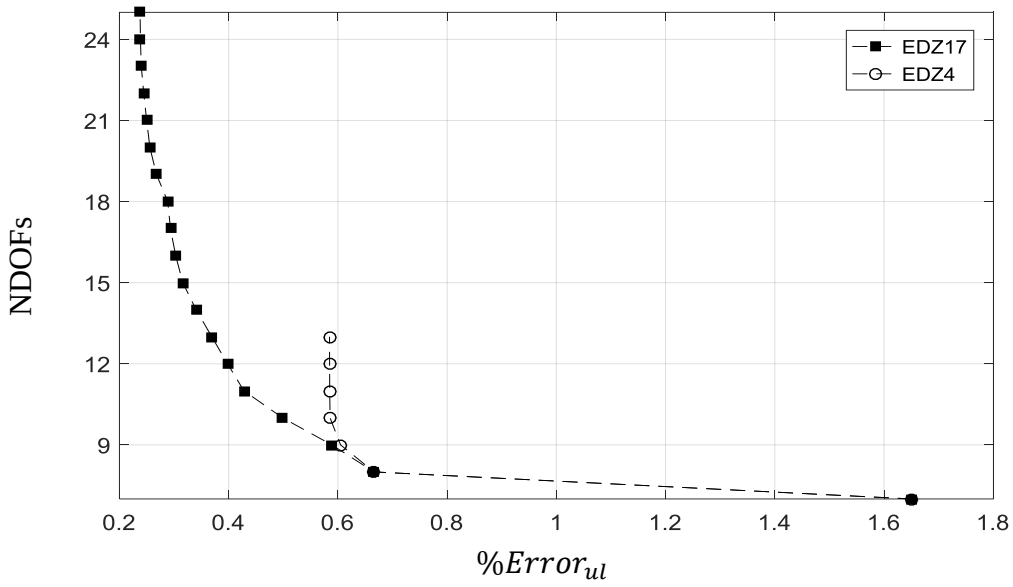

(b) $^{a}/_{h}$ = 20

Figure 6. Displacement and stress distributions along the thickness, 0º/90º/0º, $^{a}/_{h}$ = 5.

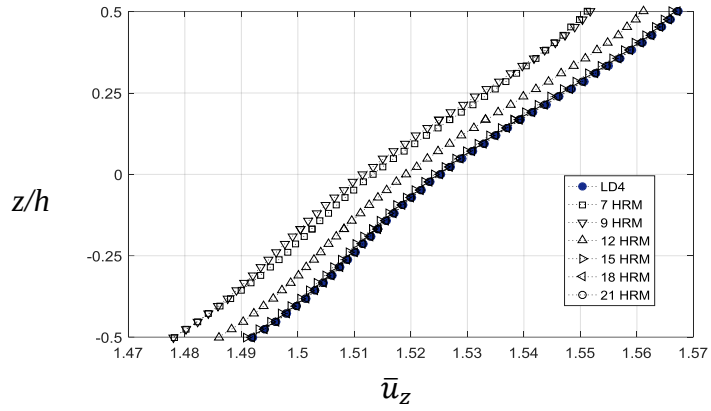

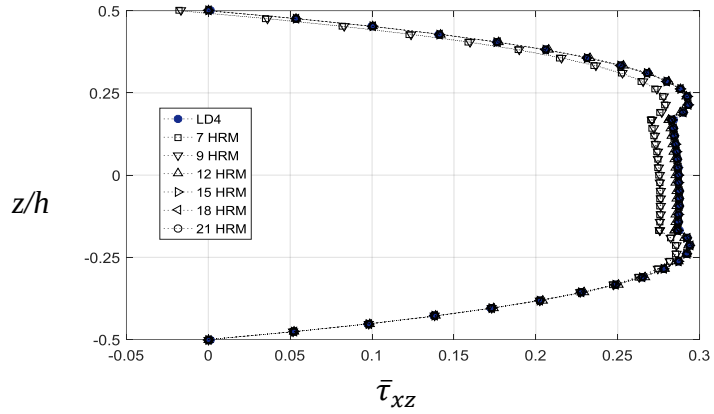

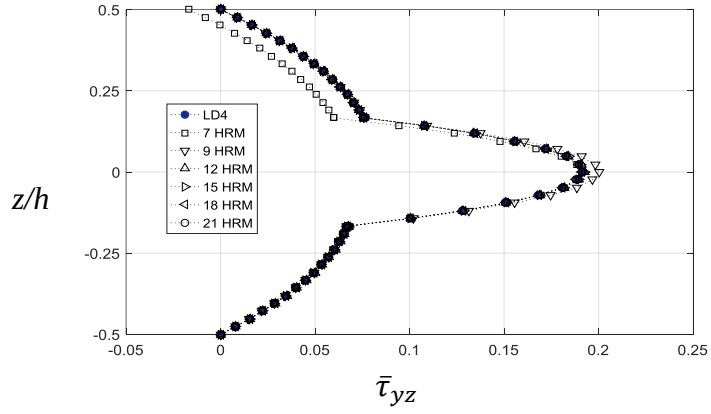

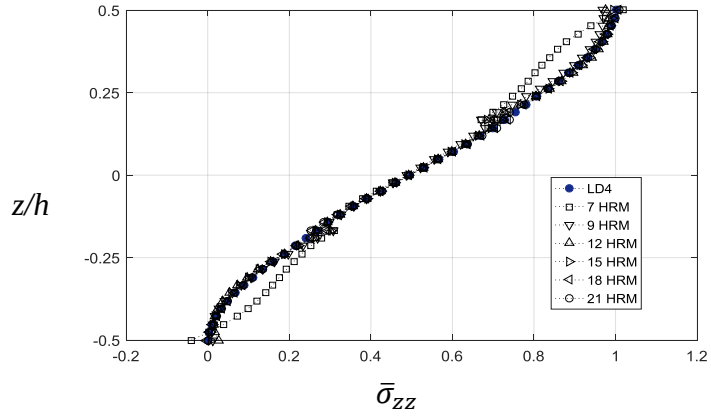

Figure 7. Displacement and stress distributions along the thickness, 0º/90º/0º, $^{a}/_{h}$ = 20.

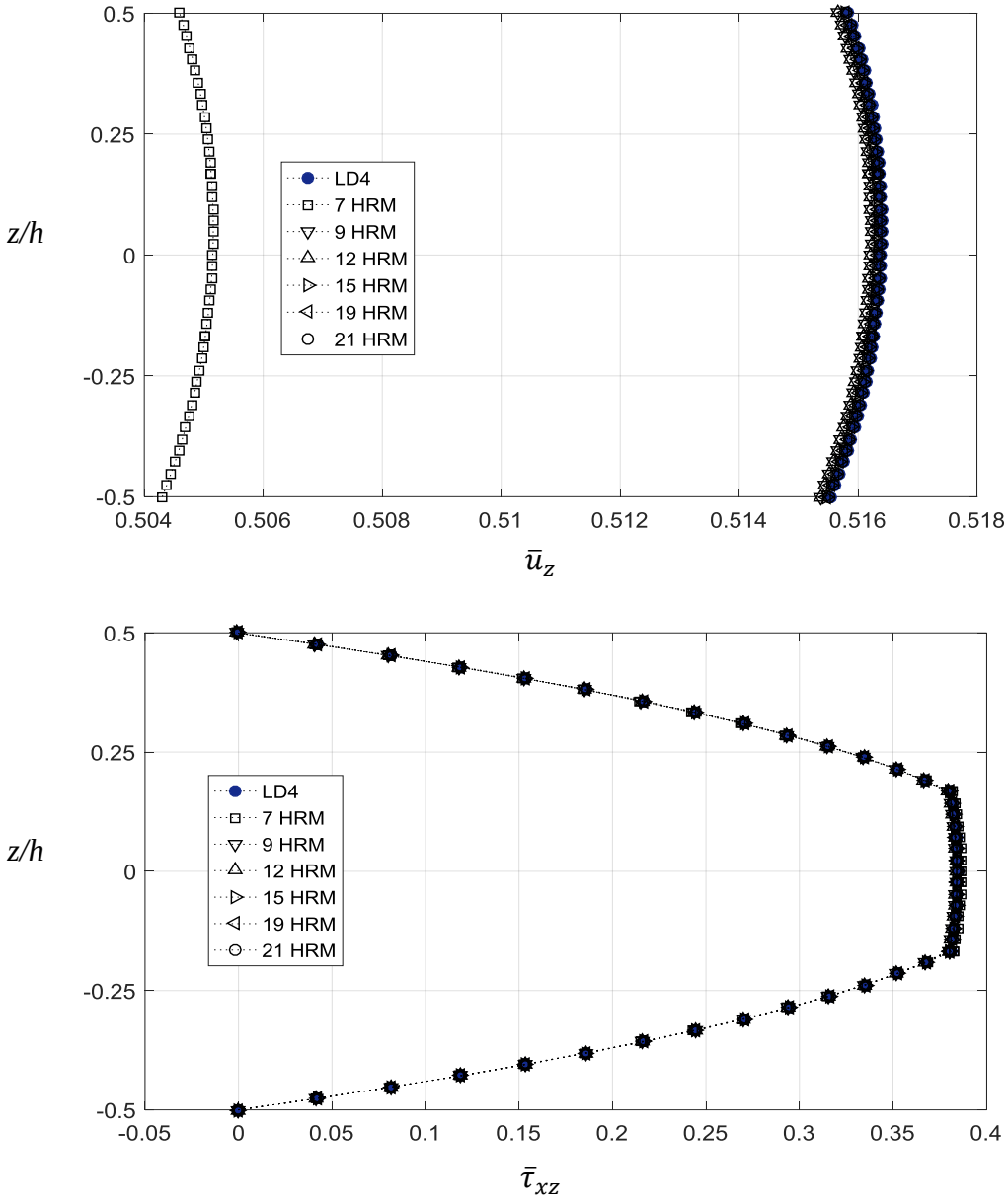

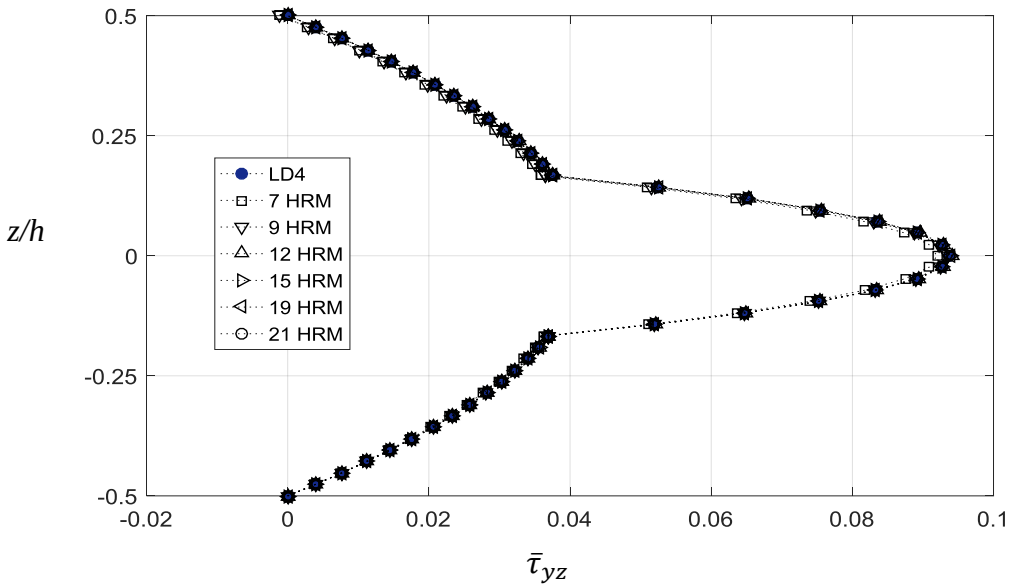
0.5
0.25
0
-0.25
-0.5
z/h
-0.02
0
0.02
0.04
0.06
0.08
0.1
$\bar{\tau}_{yz}$
LD4
7 HRM
9 HRM
12 HRM
15 HRM
19 HRM
21 HRM

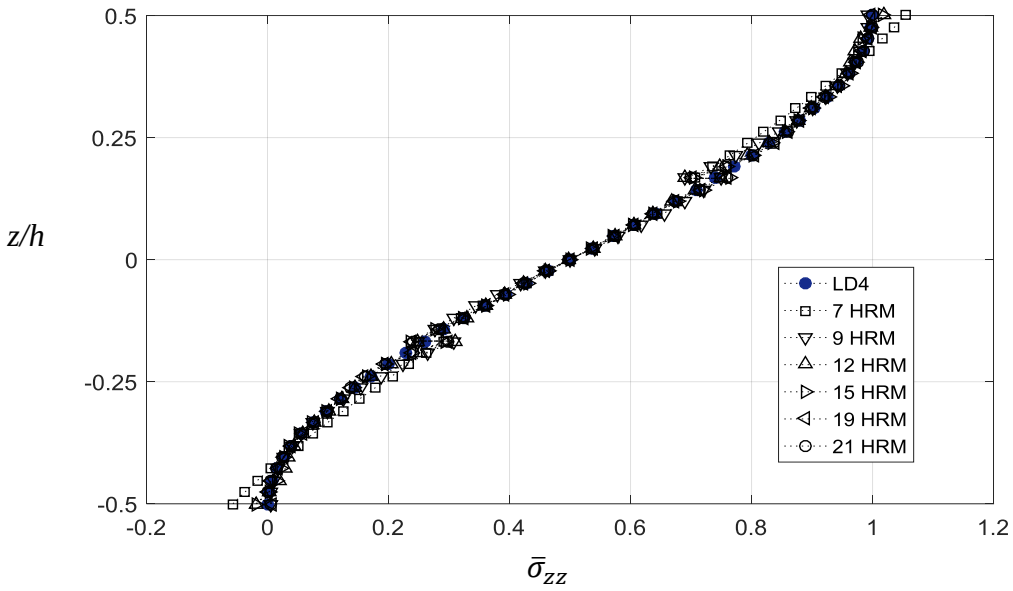
0.5
0.25
0
-0.25
-0.5
z/h
-0.2
0
0.2
0.4
0.6
0.8
1
1.2
$\bar{\sigma}_{zz}$
LD4
7 HRM
9 HRM
12 HRM
15 HRM
19 HRM
21 HRM

Figure 8. BTDs for 0º/90º, (a) $^{a}/_{h}$ = 5, (b) $^{a}/_{h}$ = 20.

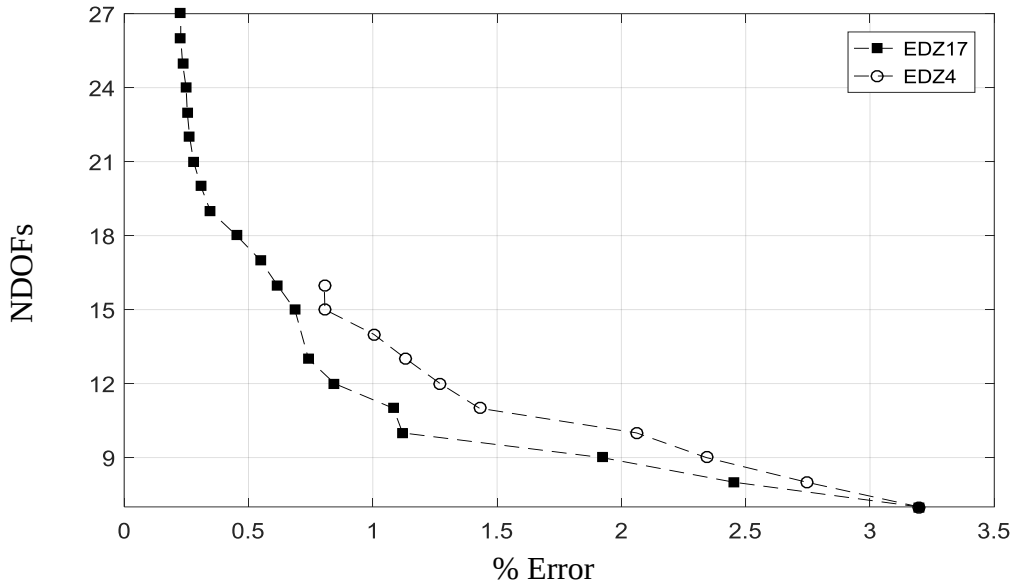

(a) $^{a}/_{h}$ = 5

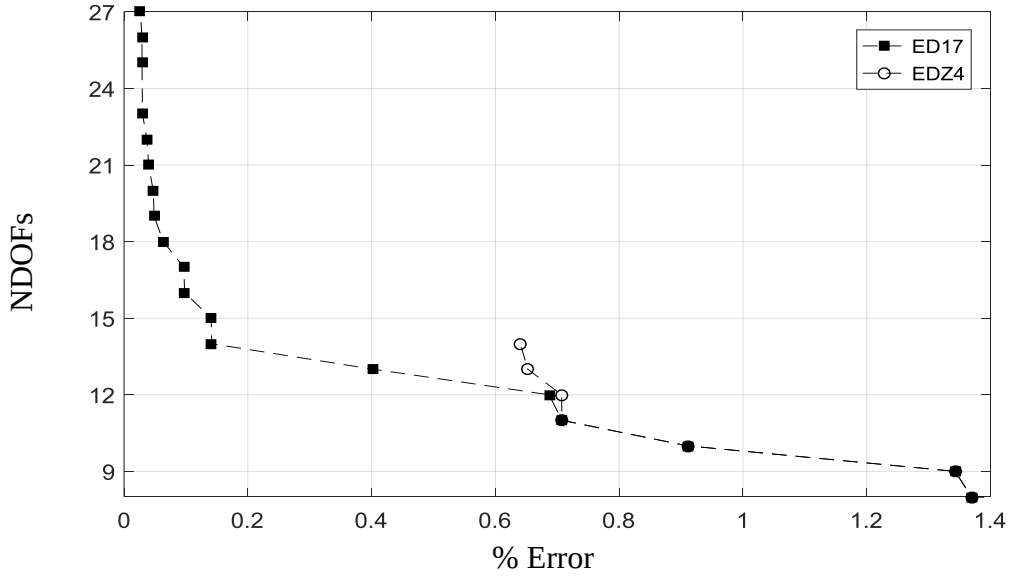

(b) $^{a}/_{h}$ = 20

Figure 9. Displacement and stress distributions along the thickness, 0º/90º, $^{a}/_{h}$ = 5.

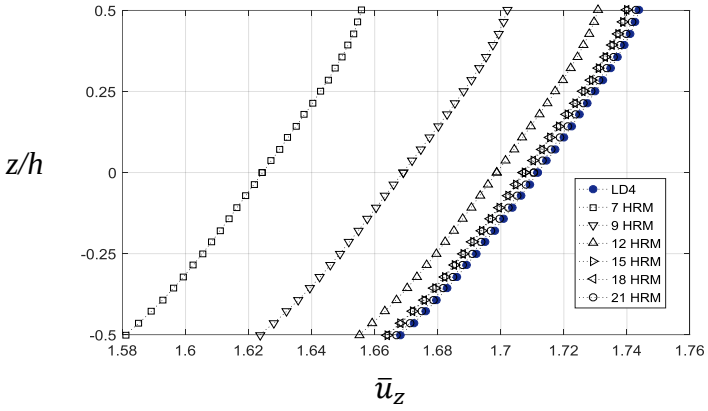

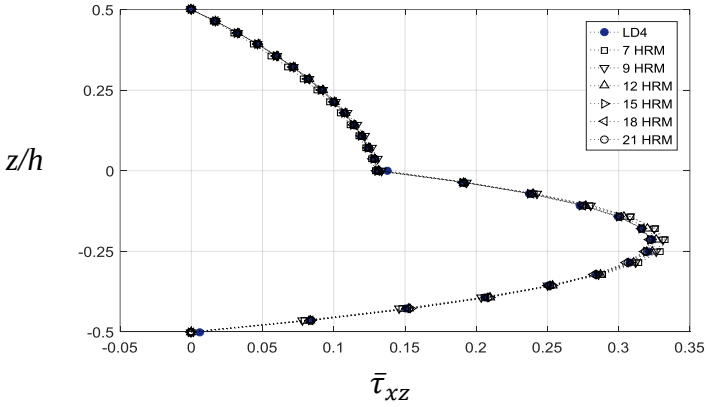

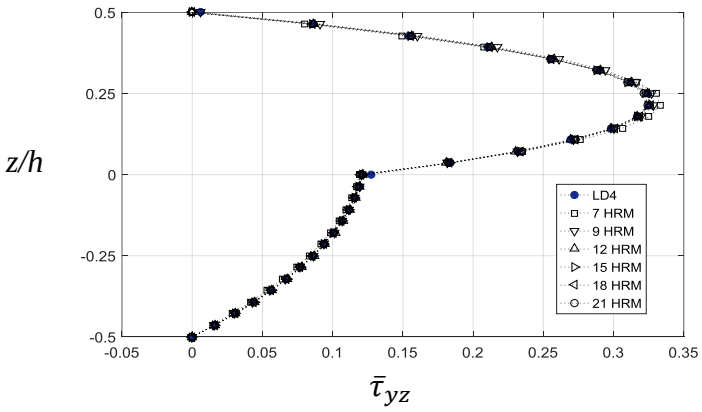

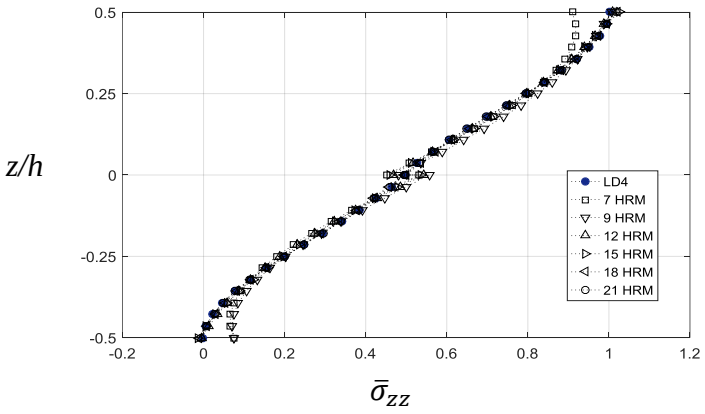

Figure 10. Displacement and stress distributions along the thickness, 0º/90º, $^{a}/_{h}$ = 20.

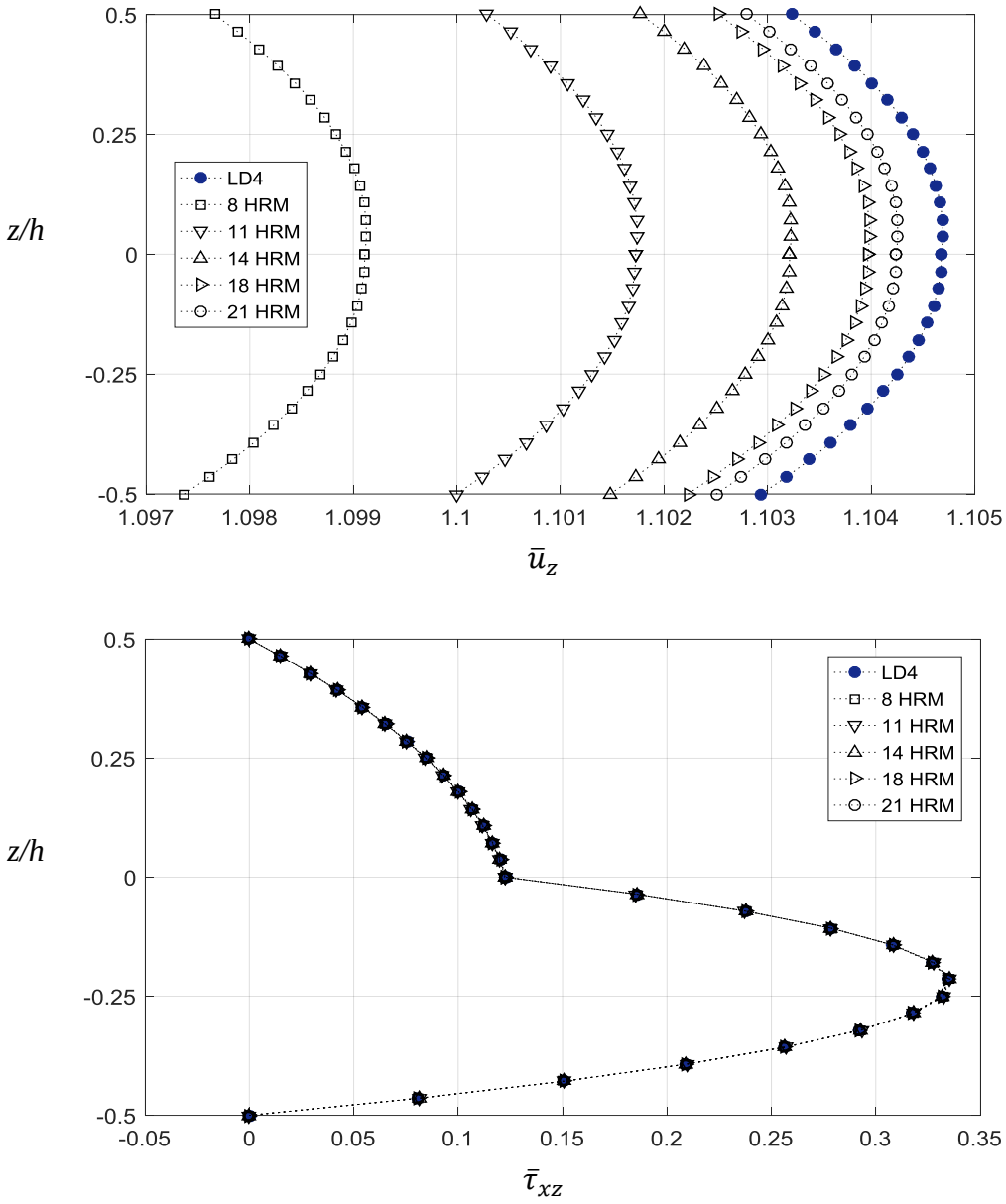

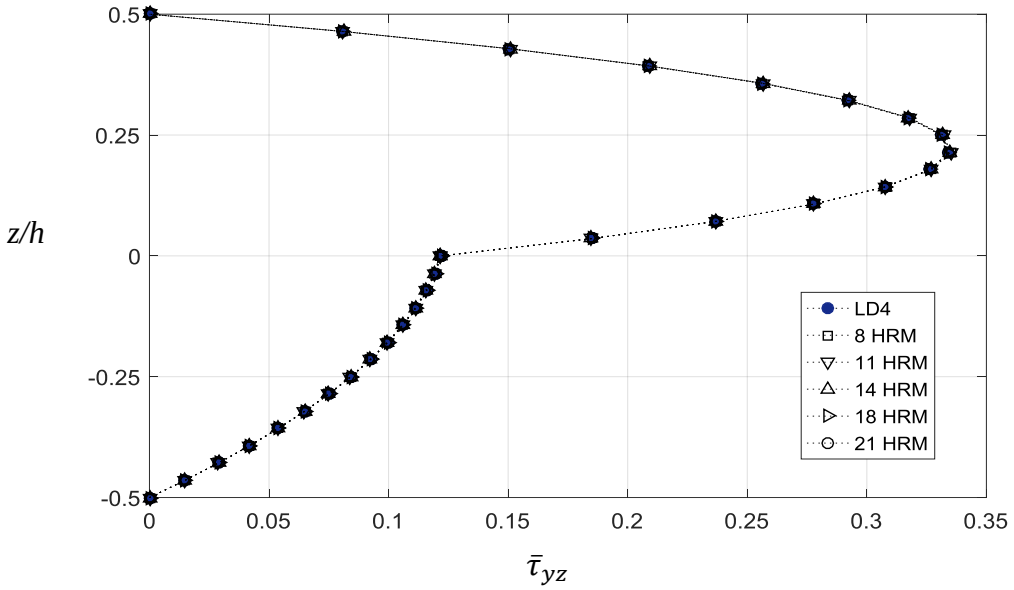
z/h
0.5
0.25
0
-0.25
-0.5
0
0.05
0.1
0.15
0.2
0.25
0.3
0.35
$\bar{\tau}_{yz}$
LD4
8 HRM
11 HRM
14 HRM
18 HRM
21 HRM

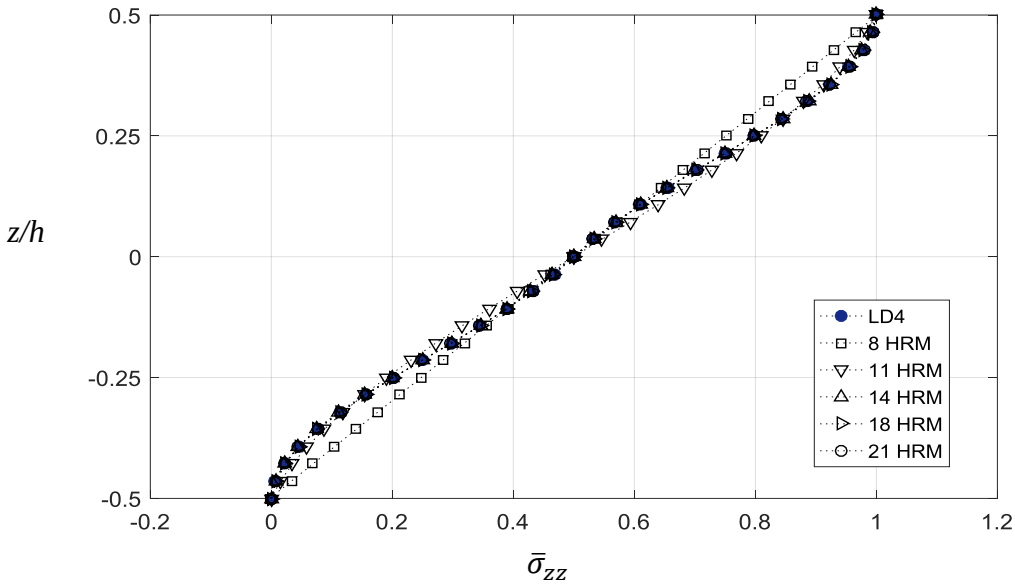
z/h
0.5
0.25
0
-0.25
-0.5
-0.2
0
0.2
0.4
0.6
0.8
1
1.2
$\bar{\sigma}_{zz}$
LD4
8 HRM
11 HRM
14 HRM
18 HRM
21 HRM

Figure 11. BTDs for 0º/90º/90º/0º, (a) $^{a}/_{h}$ = 5, (b) $^{a}/_{h}$ = 20.

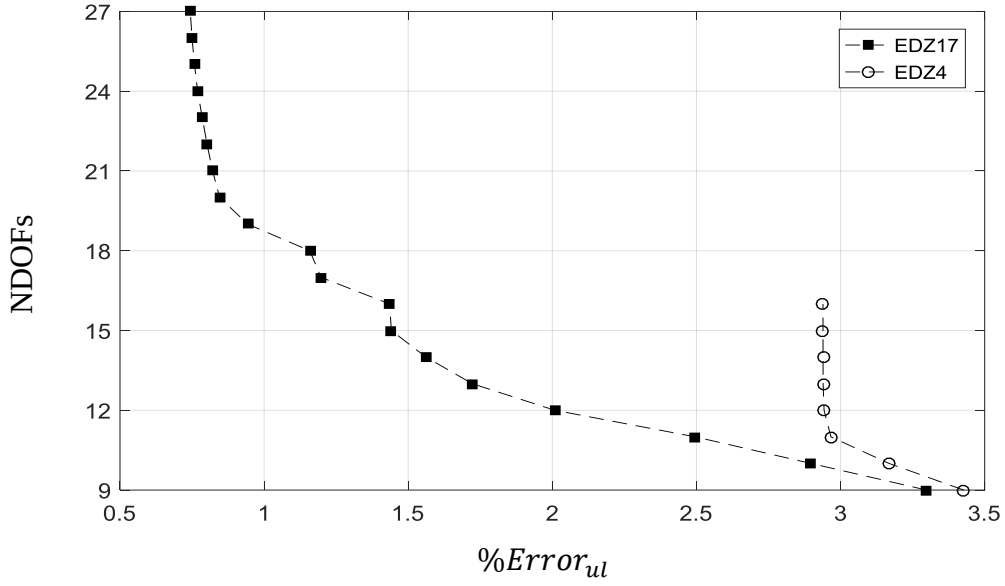

(a) $^{a}/_{h}$ = 5

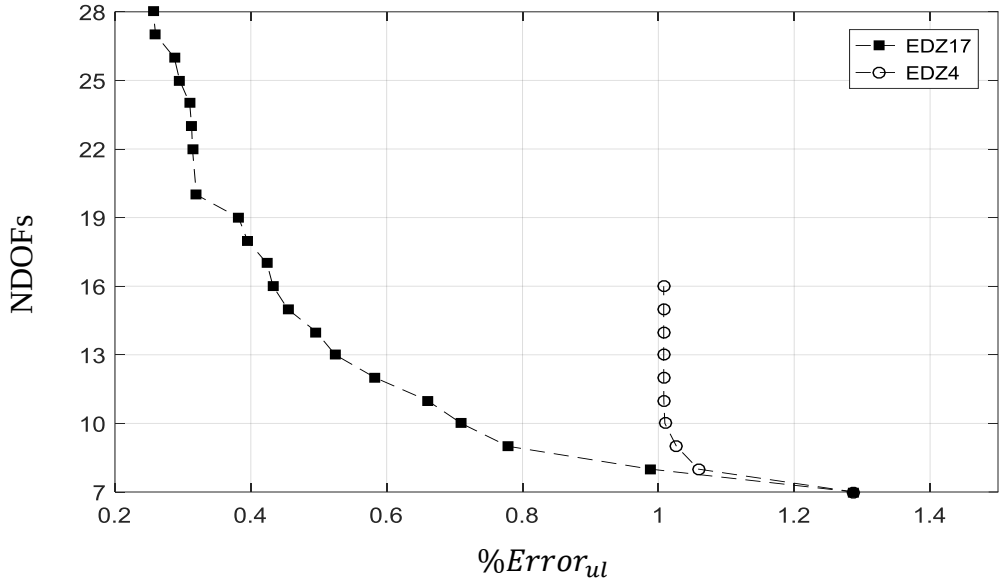

(b) $^{a}/_{h}$ = 20

Figure 12. Displacement and stress distributions along the thickness, 0º/90º/90º/0º, $^{a}/_{h}$ = 5.

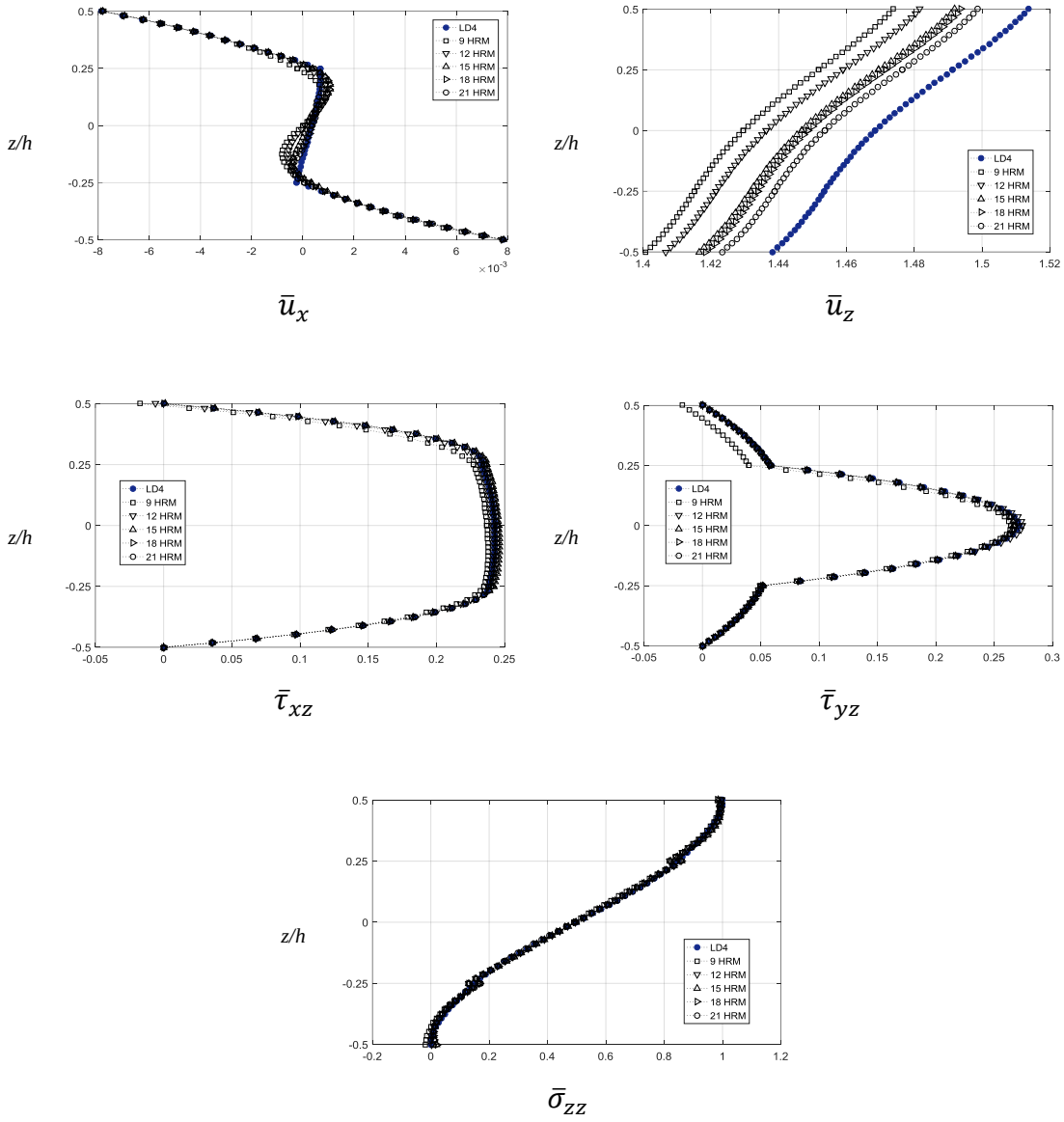

Figure 13. Displacement and stress distributions along the thickness, 0º/90º/90º/0º, $^{a}/_{h}$ = 20.

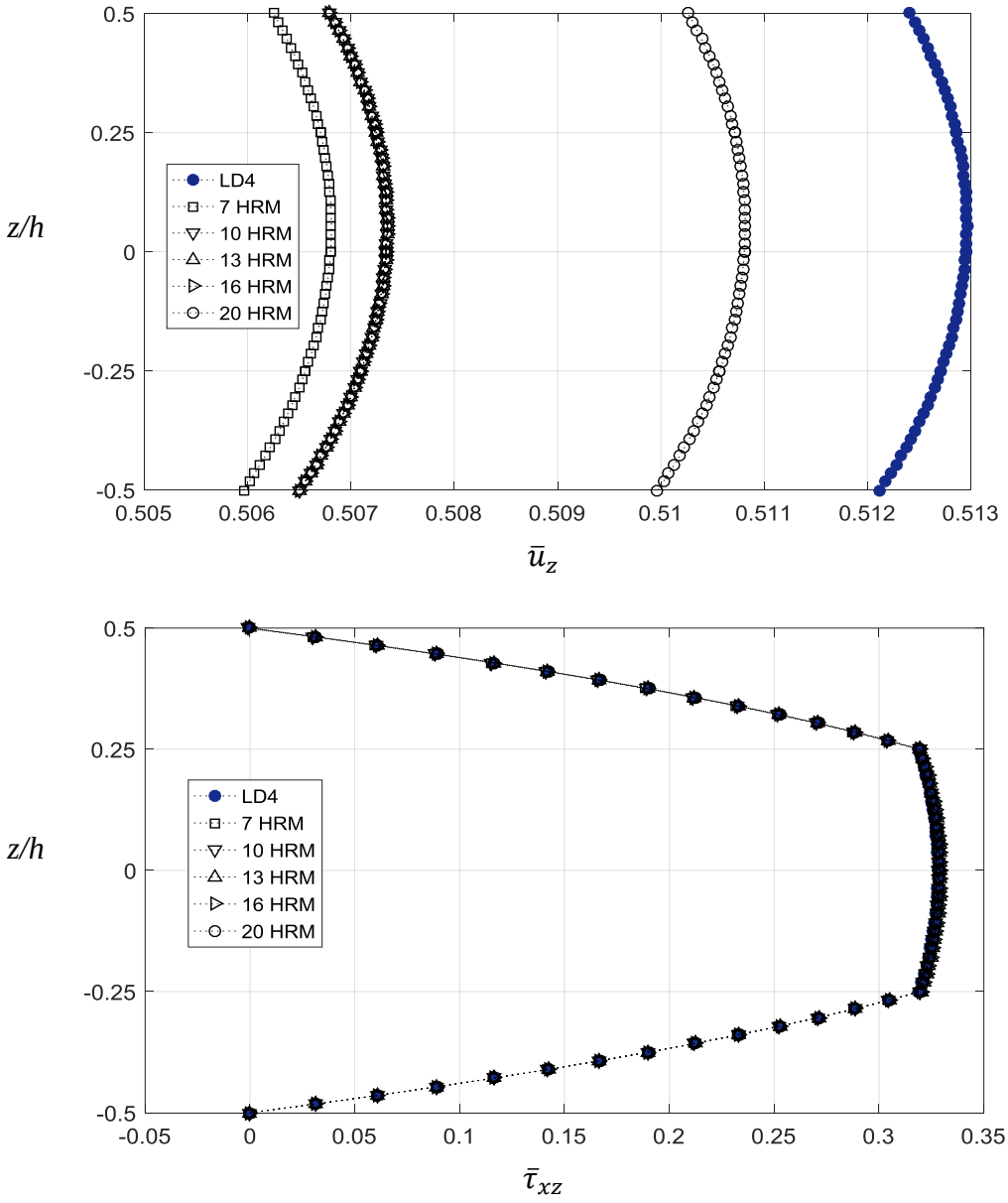

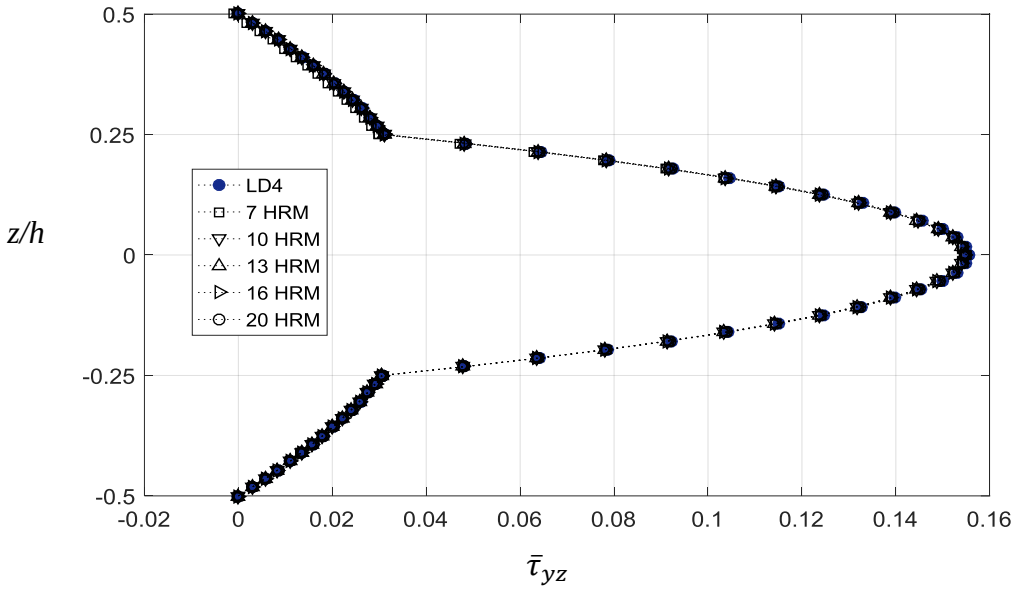
0.5
0.25
0
-0.25
-0.5
z/h
LD4
7 HRM
10 HRM
13 HRM
16 HRM
20 HRM
-0.02
0
0.02
0.04
0.06
0.08
0.1
0.12
0.14
0.16
$\bar{\tau}_{yz}$

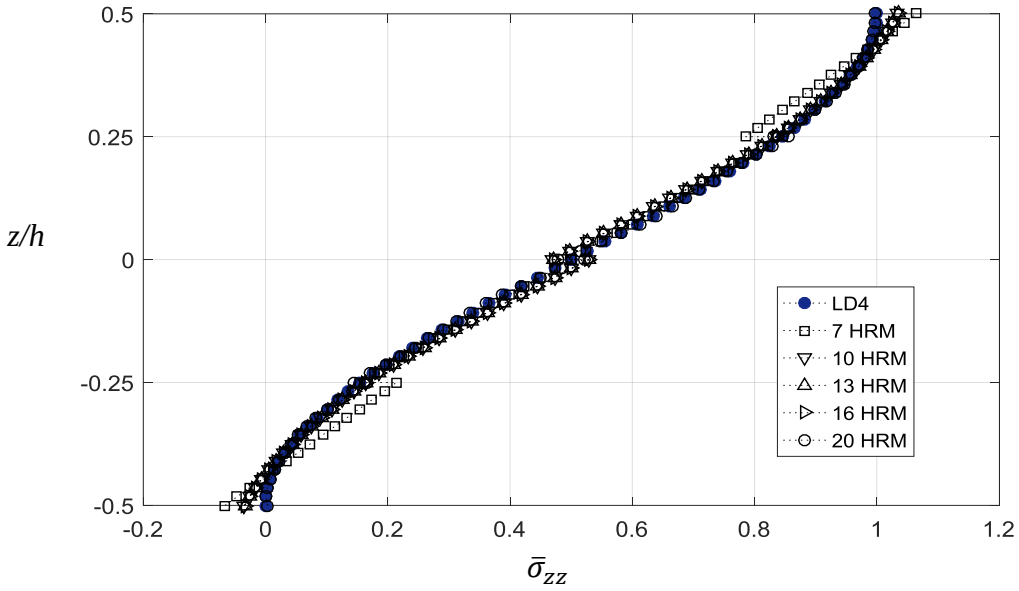
0.5
0.25
0
-0.25
-0.5
z/h
LD4
7 HRM
10 HRM
13 HRM
16 HRM
20 HRM
-0.2
0
0.2
0.4
0.6
0.8
1
1.2
$\bar{\sigma}_{zz}$